THESIS FOR THE DEGREE OF DOCTOR OF PHILOSOPHY

Molecular observations of obscured galaxy nuclei

NIKLAS FALSTAD

CHALMERS

Department of Space, Earth and Environment
CHALMERS UNIVERSITY OF TECHNOLOGY
Göteborg, Sweden 2017

Molecular observations of obscured galaxy nuclei
NIKLAS FALSTAD

ISBN 978-91-7597-677-8
Doktorsavhandlingar vid Chalmers tekniska högskola
Ny serie nr 4358.
ISSN 0346-718X

Department of Space, Earth and Environment
Chalmers University of Technology
SE–412 96 Göteborg, Sweden
Phone: +46 (0)31–772 1000

Printed by Chalmers Reproservice
Chalmers University of Technology
Göteborg, Sweden 2017

Molecular observations of obscured galaxy nuclei

NIKLAS FALSTAD
Department of Space, Earth and Environment
Chalmers University of Technology

Abstract

It is becoming evident that some (ultra)luminous infrared galaxies ((U)LIRGs) contain compact obscured nuclei (CONs) where luminosities in excess of 10^9 $L_\odot$ emerge from inside dusty regions smaller than 100 pc in diameter. Due to the obscured nature of these objects, their inner regions are hidden from examination using optical or infrared lines. In addition, extreme column densities ($\gtrsim 10^{24}$ cm^{-2}) towards the central regions might render them heavily Compton-thick, blocking even X-rays originating in the nuclei. It is nevertheless important to reveal and understand the nature of the sources behind the high luminosities, as well as their connection to the host galaxies, as this may aid our understanding of galaxy evolution and the connection between starbursts and active galactic nuclei (AGN).

This thesis describes observational efforts at far-infrared, (sub)millimeter, and radio wavelengths, with a focus on molecular line emission and absorption, combined with theoretical work, to investigate the central regions of CONs. Far-infrared and submillimeter observations of the LIRGs Zw 049.057 and Arp 299A, and the ULIRG IRAS 13120-5453 obtained with the *Herschel* Space Observatory as well as interferometric (sub)millimeter and radio observations of Zw 049.057 obtained with current state of the art interferometers are presented. Based on the *Herschel* observations, which targeted spectral lines of water (H_2O) and hydroxyl (OH), we construct radiative transfer models in order to constrain the physical conditions in the three galaxies. In this way we find that both Zw 049.057 and Arp 299A host compact obscured nuclei, while IRAS 13120-5453 does not. It is however still difficult to determine the nature of the power sources in the two CONs, and high angular resolution observations of tracers that are able to probe highly enshrouded and compact regions are definitely required in order to do this. The *Herschel* observations also included signatures of inflowing gas in both Zw 049.057 and Arp 299A as well as a tentative signature of outflowing gas in Zw 049.057. The interferometric follow-up observations of Zw 049.057 further revealed a nuclear molecular outflow detected both in radio absorption lines of OH and (sub)millimeter emission lines of CO. We interpret this combination of in- and outflowing gas motions close to the nucleus as evidence that these objects are in a short transition phase, close to the onset of strong feedback from the nucleus. The study of CONs might thus be essential for our understanding of the global evolution of galaxies.

Keywords: Galaxies: nuclei – Galaxies: ISM – ISM: molecules – Infrared: galaxies – Submillimeter: galaxies

Research contributions

This thesis is based on the work contained in the following four papers:

I **N. Falstad**, E. González-Alfonso, S. Aalto, P.P. van der Werf, J. Fischer, S. Veilleux, M. Meléndez, D. Farrah & H. A. Smith:
Herschel spectroscopic observations of the compact obscured nucleus in Zw 049.057
Astronomy & Astrophysics, 580, 52 (2015)

II **N. Falstad**, E. González-Alfonso, S. Aalto & J. Fischer:
Inflowing gas onto a compact obscured nucleus in Arp 299A: Herschel spectroscopic studies of H_2O and OH
Astronomy & Astrophysics, 597, 105 (2017)

III G. C. Privon, S. Aalto, **N. Falstad**, S. Muller, E. González-Alfonso, K. Sliwa, E. Treister, F. Costagliola, L. Armus, A. S. Evans, S. García-Burillo, T. Izumi, K. Sakamoto & P. van der Werf:
The dense molecular gas and nuclear activity in the ULIRG IRAS 13120-5453
The Astrophysical Journal , 835, 213 (2017)

IV **N. Falstad**, S. Aalto, J. G. Mangum, F. Costagliola, J. S. Gallagher, E. González-Alfonso, K. Sakamoto, S. König, S. Muller, A. S. Evans & G. C. Privon:
Hidden molecular outflow in the LIRG Zw 049.057
Accepted for publication in Astronomy & Astrophysics

I have also participated in the following papers not included in the thesis:

i A. B. Romeo & **N. Falstad**:
A simple and accurate approximation for the Q stability parameter in multicomponent and realistically thick discs
Monthly Notices of the Royal Astronomical Society, 433, 1389 (2013)

ii E. González-Alfonso, J. Fischer, J. Graciá-Carpio, **N. Falstad**, E. Sturm, M. Meléndez, H. W. W. Spoon, A. Verma, R. I. Davies, D. Lutz, S. Aalto, E. Polisensky, A. Poglitsch, S. Veilleux & A. Contursi:
The Mrk 231 molecular outflow as seen in OH
Astronomy & Astrophysics, 561, 27 (2014)

iii E. González-Alfonso, J. Fischer, S. Aalto & **N. Falstad**:
Modeling the H_2O submillimeter emission in extragalactic sources
Astronomy & Astrophysics, 567, 91 (2014)

iv E. González-Alfonso, J. Fischer, E. Sturm, J. Graciá-Carpio, S. Veilleux, M. Meléndez, D. Lutz, A. Poglitsch, S. Aalto, **N. Falstad**, H. W. W. Spoon, D. Farrah, A. Blasco, C. Henkel, A. Contursi, A. Verma, M. Spaans, H. A. Smith, M. L. N. Ashby, S. Hailey-Dunsheath, S. García-Burillo, J. Martín-Pintado, P. van der Werf, R. Meijerink & R. Genzel:
High-lying OH Absorption, [C II] Deficits, and Extreme L_{FIR}/M_{H2} Ratios in Galaxies
The Astrophysical Journal, 800, 69 (2015)

v J. E. Lindberg, S. Aalto, S. Muller, I. Martí-Vidal, **N. Falstad**, F. Costagliola, C. Henkel, P. van der Werf, S. García-Burillo & E. González-Alfonso:
Evidence for a chemically differentiated outflow in Mrk 231
Astronomy & Astrophysics, 587, 15 (2016)

vi C. Yang, A. Omont, A. Beelen, E. González-Alfonso, R. Neri, Y. Gao, P. van der Werf, A. Weiß, R. Gavazzi, **N. Falstad**, A. J. Baker, R. S. Bussmann, A. Cooray, P. Cox, H. Dannerbauer, S. Dye, M. Guélin, R. Ivison, M. Krips, M. Lehnert, M. J. Michałowski, D. A. Riechers, M. Spaans & E. Valiante:
Submillimeter H_2O and H_2O^+emission in lensed ultra- and hyper-luminous infrared galaxies at $z \sim 2-4$
Astronomy & Astrophysics, 595, 80 (2016)

vii E. González-Alfonso, J. Fischer, H. Spoon, K. P. Stewart, M. L. N. Ashby, S. Veilleux, H. A. Smith, E. Sturm, D. Farrah, **N. Falstad**, M. Meléndez, J. Graciá-Carpio, A. W. Janssen & V. Lebouteiller:
Molecular outflows in local ULIRGs: Energetics from multi-transition OH analysis
The Astrophysical Journal, 836, 11 (2017)

viii S. Aalto, S. Muller, F. Costagliola, K. Sakamoto, J. S. Gallagher, **N. Falstad**, S. König, K. Dasyra, K. Wada, F. Combes, S. García-Burillo, L. E. Kristensen, S. Martín, P. van der Werf, A. S. Evans & J. Kotilainen:
Luminous, pc-scale CO 6-5 emission in the obscured nucleus of NGC 1377
Astronomy & Astrophysics, 608, 22 (2017)

Acknowledgements

First, I would like to thank my supervisor Susanne Aalto for her help and encouragement during my PhD studies. Thank you also to my second supervisor Eduardo González-Alfonso for helping me with radiative transfer matters. My third supervisor Sebastien Muller and my examiner Hans Olofsson also deserve a thank you for lending their critical eyes to the drafts of this thesis. A special thank you to my master's thesis supervisor Alessandro Romeo who really led me into astronomy. My many collaborators also deserve a thank you for sharing their knowledge and helping me with my work. Thank you also to all my colleagues at the observatory and Chalmers, especially my fellow PhD students, for providing such an inspiring work environment.
Finally, I would like to thank my parents and siblings for their encouragement and help during my studies. And of course my wife Jenni and our daughter Ebba, for giving me love and support whenever I needed it.

Niklas

Contents

Chapter 1

Introduction

Through the analysis of radiation that has traveled to us from distant regions of the Universe, we learn a lot about the physical and chemical conditions in the places where it originated. In some galaxies, a large portion of the emitted radiation emerges from very compact and obscured regions inside their nuclei. The obscured nature of these objects makes it hard to determine what kind of processes are responsible for the large amounts of energy emanating from their interiors. It is nevertheless important to reveal and understand the nature of the sources behind the high luminosities, as this may aid our understanding of galaxy evolution as well as the connection between starbursts and active galactic nuclei (AGN). That is the topic of this thesis. Based on observations of obscured galaxy nuclei, we try to make models of their dusty interiors in an effort to understand what drives them.

The rest of this introductory chapter is devoted to a brief introduction to the interstellar medium and a basic description of molecular excitation and radiative transfer, concepts that are particularly important in the later parts of the thesis. In Chapter 2 we give an account of the compact obscured nuclei that are the topic of this thesis, starting with a brief discussion of their potential power sources, continuing with a short account of the host galaxies in which they are found, and finally concluding with a discussion of the objects themselves. Chapter 3 then contains a discussion of two ways of studying these very compact and dust-obscured nuclei. Finally, in Chapter 4 we give a short introduction to each of the four appended papers.

1.1 The interstellar medium

General references: Tielens (2010); Omont (2007)

Although stars make up most of the visible mass of galaxies, they only fill a very small fraction of the total galactic volume. Filling the void between stellar systems in galaxies is the very tenuous mix of gas and dust referred to as the interstellar medium (ISM). This is the matter from which stars are formed, but the stars themselves also influence the ISM as they inject processed stellar material as well as radiative and mechanical energy. This cyclic process drives the galactic physical and chemical evolution, and studies of the ISM are thus important to understand the history, and predict the future, of galaxies.

The ISM is a multi-phase medium where ionized, atomic, and molecular gas as well as ices and dust particles reside in a variety of different environments. By mass, most of the gas is atomic or molecular hydrogen with lesser amounts of helium and less than one percent of heavier elements. The fraction of heavier elements is however slowly increasing because of the nucleosynthesis that occurs in stars and supernovae. Dust constitutes only ~ 1 % of the total ISM mass but it is an important catalyst for the formation of molecular hydrogen (Hollenbach & Salpeter, 1971) and the major source of opacity for non-ionizing photons. Dust grains are efficient absorbers at ultraviolet (UV) and visual wavelengths, and by re-radiating the absorbed light in the infrared, dust strongly affects the spectral energy distribution of entire galaxies. The grains are also able to lock up a significant fraction of the heavier elements of the ISM; and provide a surface for other species to freeze out onto, combine into molecular ices, and return to the gas-phase through evaporation and sputtering in warm regions and shocks, respectively.

1.1.1 Molecules

Molecules play an immensely important role in the ISM as the dense cores of molecular clouds are the sites of star formation. Due to the large fraction of hydrogen in the ISM, the bulk of the molecular gas is in H_2, with less than 1% (by mass) of the gas in other molecules. Molecular hydrogen is however hard to observe due to its lack of a permanent dipole moment and the large spacing between its rotational energy levels (rotational levels are discussed in Sect. 1.2.2). As a consequence, the upper level of the lowest H_2 rotational line lies at ~ 500 K above the ground state, much higher than the typical temperature of molecular clouds. In order to study the molecular gas we must therefore rely on observations of other molecules.

A common tracer of molecular gas is carbon monoxide (CO), the second most abundant molecular species in the ISM, with a typical abundance rela-

tive to H_2 of $10^{-5}-10^{-4}$. It has closely spaced rotational energy levels with the lowest excited level at about 5.5 K and is thus easily excited even in cold environments. An additional advantage is that the three lowest rotational transitions are located at wavelengths where the atmospheric transmission is good, and therefore are observable using ground-based telescopes. However, because of its high abundance, the main isotopologue $^{12}C^{16}O$ easily becomes optically thick in its low-lying transitions, meaning that the observed emission is not sensitive to the total column of gas. This obstacle can be overcome by observing less abundant variants like $^{13}C^{16}O$ or $^{12}C^{18}O$. The low-lying CO lines are tracing gas with moderate density. Molecules like hydrogen cyanide (HCN) and the formyl ion (HCO^+) have higher dipole moments and their radiative decay to lower states is therefore faster than for CO. Because of this they do not thermalize (and saturate) in medium-density gas, and the bulk of the emission will originate in denser gas.

Of special importance in this thesis are the light hydrides OH and H_2O. These molecules have a plethora of lines at far-infrared and, in the case of H_2O, submillimeter wavelengths. The high dipole moments of these species, together with the fact that the bulk of the thermal dust emission from galaxies is emitted in the far-IR, make these transitions sensitive to radiative excitation by warm dust emission and they are thus well suited to probe the physical conditions in the nuclei of dusty galaxies. Due to atmospheric absorption, the rest frequencies of these lines are inaccessible with ground-based telescopes. Space-based facilities are therefore required in order to observe them in sources at low redshift. H_2O and OH are treated in more detail in Sect. 3.1.2.

1.1.2 Dust

Although it contributes only a small fraction of the total mass, dust is an important constituent of the ISM. The surfaces of dust grains provide a place for particles to accrete and react with each other, thus acting as an important catalyst in the formation of molecules, especially H_2 that cannot be formed efficiently in the gas phase (e.g., Gould & Salpeter, 1963). Accretion onto, and desorption from, grain mantles also regulate the gas phase abundances of different species. The most important property of dust in the context of this thesis is however its ability to obscure an embedded power source and to shift its spectral energy distribution (SED) to far-infrared wavelengths.

The exact composition of the dust grains is not well known, but the presence of some important constituents has been inferred based on spectral features identified in observations of dust absorption, scattering, and emission: a strong feature at 2175 Å is attributed to graphite while broad features at 9.7 and 18 μm indicate the presence of amorphous silicates. If the grain constituents are known, the observed wavelength-dependence of dust extinction can be used to

derive the size distribution of the dust grains. The most popular one is the so called Mathis-Rumpl-Nordsieck (MRN) distribution first suggested by Mathis et al. (1977). In this model, graphite and silicate grains have a power-law size distribution with $dn/da \propto a^{-3.5}$ where $n(a)$ is the number of particles of size a between 0.005 and 1 μm for graphite grains and between 0.025 and 0.25 μm for silicate grains.

1.2 Molecular emission and absorption

General references: Rybicki & Lightman (1979); Tielens (2010); Wilson et al. (2009)

Molecules, unlike single atoms, consist of multiple nuclei which are tightly bound together but can move with respect to each other. In addition to the electronic states seen in atoms, molecules also exhibit vibrational states involving stretching and bending of the bonds between the nuclei, as well as rotational states involving rotation around some axis. The molecule is thus a more complex system whose internal energy depends on a combination of the electronic, vibrational and rotational energy states. Fortunately, due to the much greater mass of the nuclei as compared to the electrons (a mass ratio of $M/m \sim 10^4$), the electrons are much faster and can be considered to adjust instantly to any changes in the positions of the nuclei. In this approximation, known as the Born-Oppenheimer approximation, the electronic and nuclear motions can then be treated separately. Additional approximations can then be made to separate the vibrational and rotational motions of the nuclei and write the total internal energy as a sum of the various energies, which are in the approximate ratios $1 : \sqrt{\frac{m}{M}} : \frac{m}{M}$ for the electronic, vibrational, and rotational states. Through transitions between different energy states the molecule can absorb or emit radiation at specific wavelengths that are determined by the energy difference between the involved states.

This thesis is mainly focused on the transitions that involve the lowest energies, those between rotational energy states, typically corresponding to lines in the far-infrared to the millimeter range of the electromagnetic spectrum. Parts of the thesis are also based on rotational transitions within vibrationally excited states, as well as transitions between hyperfine levels within rotational states. The following subsections contain a brief introduction to the energies involved in vibrational and rotational states as well as transitions between these states.

1.2.1 Vibrational states

Molecular vibrations involve stretching and bending of the bonds between the nuclei of the molecule. To a first approximation, this movement can be charac-

terized as a harmonic oscillator with discrete energy levels given by:

$$E_{\text{vib}} = \hbar\omega(v + \frac{1}{2}), \tag{1.1}$$

where v is the vibrational quantum number and ω is the angular frequency of the vibration. The electric dipole allowed vibrational transitions are those with $\Delta v = \pm 1$, and for a transition between state v and $v - 1$ the energy difference in this simple approximation is

$$\Delta E_{\text{vib}} = \hbar\omega. \tag{1.2}$$

This is independent of the vibrational quantum number v and consecutive states are equally spaced in energy in the harmonic oscillator approximation. In reality, the potential is anharmonic and this approximation is only good close to the bottom of the potential well. The effect of the anharmonicity is to slightly decrease the energy difference of the vibrational levels as the vibrational quantum number increases.

1.2.2 Rotational states

In the simplest case, for a rigid diatomic or linear polyatomic molecule in a $^1\Sigma$ electronic state, that is, with no electronic angular momentum or spin, the rotational energy levels are given by

$$E_{\text{rot}} = B_{\text{e}} J(J + 1), \tag{1.3}$$

where J is the rotational quantum number and B_{e} is the rotational constant which is defined as

$$B_{\text{e}} = \frac{\hbar^2}{2\Theta_{\text{e}}}, \tag{1.4}$$

where Θ_{e} is the moment of inertia of the molecule. The electric dipole allowed rotational transitions are those with $\Delta J = \pm 1$ and for a transition between state J and $J - 1$ the energy difference is

$$\Delta E_{\text{rot}} = 2B_{\text{e}} J. \tag{1.5}$$

Thus, in this simple case, the energy difference is proportional to J and the spectral lines will be equally spaced in frequency. In practice, molecules are not rigid, and additional terms must be included to account for the stretching of the molecule due to centrifugal forces. The effect of the stretching is to increase the moment of inertia as the rotational quantum number increases, and thus decrease the energy difference between levels. The lowest rotational levels of the linear molecule HCN are shown in the left panel of Fig. 1.1.

For non-linear molecules, the situation is a bit more complicated. An arbitrary molecule can be described by its three principal moments of inertia: Θ_A,

Θ_B, and Θ_C where the axes are generally chosen so that $\Theta_A \leq \Theta_B \leq \Theta_C$. If all three moments of inertia are equal the molecule is referred to as a spherical top, if two moments of inertia are equal it is a symmetric top, and if no two moments of inertia are equal the molecule is an asymmetric top. Symmetric tops can be further divided into prolate (cigar-shaped) tops where $\Theta_A < \Theta_B = \Theta_C$ and oblate (disk-shaped) tops where $\Theta_A = \Theta_B < \Theta_C$.

The rotational state of a symmetric top can be described by the rotational quantum number J and its projection onto the axis of symmetry, K. The allowed radiative transitions for symmetric top molecules are those with $\Delta J = \pm 1$ and $\Delta K = 0$. Transitions with $\Delta K \neq 0$ are however allowed for collisions and the populations of the different K-ladders are thus determined by collisional excitation, making symmetric tops useful as probes of the gas temperature. The energy of each state in a symmetric top is given by

$$E_{\text{rot}} = BJ(J+1) + (A-B)K^2, \tag{1.6}$$

for a prolate molecule and

$$E_{\text{rot}} = BJ(J+1) + (C-B)K^2, \tag{1.7}$$

for an oblate molecule. A, B and C are here the rotational constants given by

$$A = \frac{\hbar^2}{2\Theta_A}, \tag{1.8}$$

$$B = \frac{\hbar^2}{2\Theta_B}, \tag{1.9}$$

$$C = \frac{\hbar^2}{2\Theta_C}. \tag{1.10}$$

As the energy of a particular state depends on K^2, the sign of K does not matter, and all states with $|K| > 0$ are doubly degenerate. The energy level diagram of the prolate symmetric top NH_3 is shown in the right panel of Fig. 1.1.

For symmetric top molecules, both J and K are time-invariable and thus good quantum numbers. For asymmetric top molecules this is still true for J, but they have no internal molecular axes with a time-invariable component of the angular momentum. One way to describe asymmetric top molecules is to use the rotational quantum number J and the approximate quantum numbers K_a, for the limiting prolate top, and K_c, for the limiting oblate top. In this case there are no simple expressions to describe the energy levels, and the deviation from symmetry lifts the degeneracy in energy seen in symmetric top molecules. One example of an asymmetric top is H_2O, whose energy level diagram is shown in the right part of Fig. 3.2 in Sect. 3.1.2.

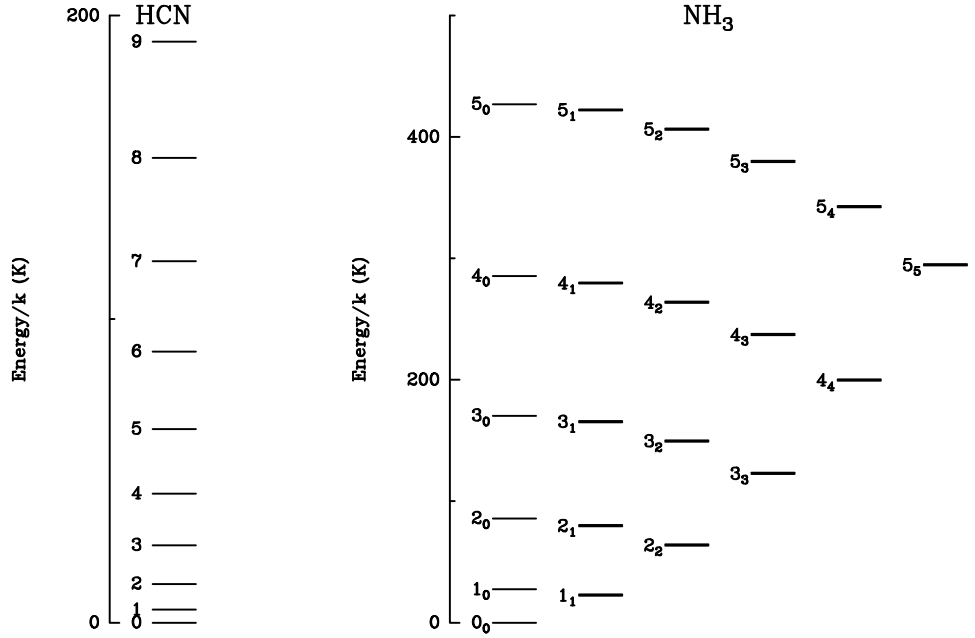

Figure 1.1: Energy level diagrams of the linear molecule HCN and the prolate symmetric top NH_3.

Lambda-doubling, orbit-spin coupling, and hyperfine splitting in OH

Although this thesis is not concerned with electronic transitions, the electronic state does affect the rotational states that are of interest here. Most molecules have a $^1\Sigma$ electronic ground state with no electronic angular momentum. Some molecules, however, do have electronic angular momentum in their ground state, for example OH with its $^2\Pi$ ($1/2$ electronic spin and ± 1 angular momentum along the molecular axis) ground state. In these molecules, the degenerate rotational energy levels are further split up due to interactions between the molecular and electronic angular momenta, so called Λ-doubling. In addition, in molecules which also have non-zero electronic spin, the electronic angular momentum along the molecular axis couples with the electronic spin. In OH, this orbit-spin coupling gives rise to the $^2\Pi_{3/2}$ and $^2\Pi_{1/2}$ splitting seen in Fig. 1.2.

For molecules with non-zero nuclear spin, further so called hyperfine splitting is introduced through the coupling of the rotational motion of the molecule to the nuclear spin I. With the introduction of the total angular momentum vector $\boldsymbol{F} = \boldsymbol{J} + \boldsymbol{I}$, the hyperfine levels can be labeled with the conserved quantum number F. The dipole allowed transitions between these levels are those with $\Delta F = 0, 1$ but not $F = 0 \rightarrow 0$. In OH, the hydrogen nucleus has a spin of $I = \frac{1}{2}$ while the oxygen nucleus has a spin of zero, leading to hyperfine splitting of

the already Λ-doubled rotational levels. The energy level diagram of the three first rotational states of the OH molecule are shown in Fig. 1.2, including Λ-doubling, orbit-spin coupling, and hyperfine splitting.

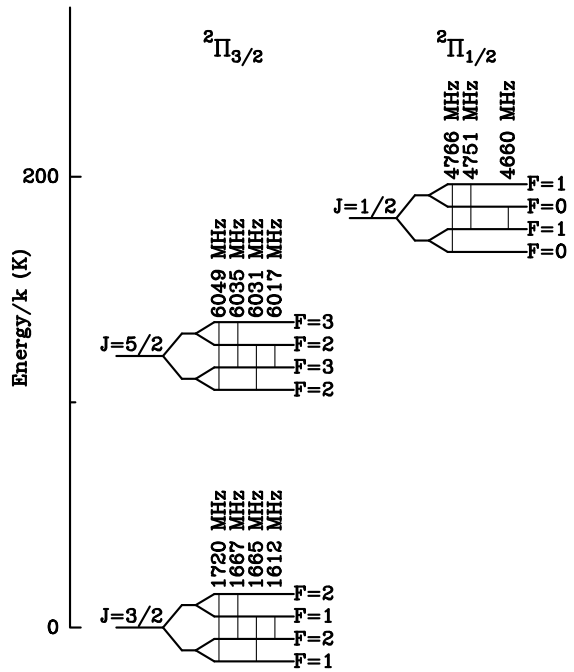

Figure 1.2: Energy diagram showing the ground and two first excited rotational states of OH. The Λ-doubling and hyperfine levels are not to scale. Transitions between hyperfine levels are indicated with lines connecting the levels in question and their frequencies are shown above the lines.

1.2.3 Excitation of states

Radiative transitions between different states occur when the molecule interacts with photons from the surrounding radiation field. A convenient way to treat these transitions is to use the Einstein coefficients. These are A_{ul} (s^{-1}), which give the probability per unit time for the spontaneous emission of a photon, and B_{ul} and B_{lu} ($J^{-1}\,m^2\,s^{-1}$), which give the probabilities per unit time per unit mean intensity for the stimulated emission or absorption of a photon, respectively. The subscripts u and l refer to the upper and lower energy levels, respectively, in each transition. The Einstein coefficients are related to each other by

$$g_l B_{lu} = g_u B_{ul} \tag{1.11}$$

and

$$A_{ul} = \frac{2h\nu^3}{c^2} B_{ul}, \tag{1.12}$$

where g_l and g_u are the statistical weights of the involved states.

Not only radiative processes affect the molecular excitation, and in a proper treatment transitions induced by collisions with other molecules must also be accounted for. The rate of collisional excitation C_{ij} from level i to level j can be expressed as $C_{ij} = nq_{ij}$ where n is the number density of the collision partner (usually H_2) and q_{ij} ($\mathrm{cm^3\,s^{-1}}$) is a collisional rate coefficient that depends on the temperature of the gas. When the time scales of chemical processes are sufficiently short, also the state-specific formation and destruction rates, F_i and D_i, must be taken into account (van der Tak et al., 2007).

If the excitation and de-excitation between levels balance in such a way that the level populations do not change with time, the system is said to be in statistical equilibrium (SE). This is usually a very good approximation in astrophysical systems as the rates for (de-)excitation are much quicker than the rates at which conditions change. With the Einstein coefficients, collision rates, and state-specific formation and destruction rates in place, we can write down the equations for statistical equilibrium:

$$\begin{aligned}\frac{\mathrm{d}n_i}{\mathrm{d}t} =& \sum_{j<i}^{N} [(n_j B_{ji} - n_i B_{ij})\bar{J}_{ij} - n_i A_{ij}] \\ &+ \sum_{j>i}^{N} [(n_j B_{ji} - n_i B_{ij})\bar{J}_{ij} + n_j A_{ji}] \\ &+ \sum_{j\neq i}^{N} [n_j C_{ji} - n_i C_{ij}] + F_i - n_i D_i = 0,\end{aligned} \tag{1.13}$$

where $\bar{J}_{ij}$ is the the intensity of the radiation field (see Sect. 1.3) averaged over all directions ($\vec{n}$) and integrated over the line profile:

$$\bar{J}_{ij} = \frac{1}{4\pi} \int I_\nu(\vec{n}) \phi_{ij}(\nu, \vec{n}) \mathrm{d}\Omega \mathrm{d}\nu. \tag{1.14}$$

In the two simple cases of two-level systems where either radiation or collisions totally dominate the excitation, the relative level populations are given by a Boltzmann distribution with a temperature related to the excitation mechanism at work. When only radiative processes affect the excitation, the relative populations are given by

$$\frac{n_u}{n_l} = \frac{g_u}{g_l} \exp\left(-\frac{h\nu_{ul}}{kT_\mathrm{b}}\right), \tag{1.15}$$

where ν_{ul} is the frequency of the transition and T_b is the brightness temperature given by

$$T_\mathrm{b} = \frac{h\nu_{ul}}{k} \frac{1}{\ln\left(\frac{2h\nu^3}{c^2 J_{ul}} + 1\right)}. \tag{1.16}$$

If on the other hand collisions totally dominate the excitation and the rates for collisional de-excitation are much higher than the Einstein A-coefficient, the relative populations are given by

$$\frac{n_u}{n_l} = \frac{g_u}{g_l} \exp\left(-\frac{h\nu_{ul}}{kT_\mathrm{K}}\right), \tag{1.17}$$

where T_K is the kinetic temperature describing the velocity distribution of the colliding particles. In general, neither process can be totally neglected and the relative populations are given by

$$\frac{n_u}{n_l} = \frac{g_u}{g_l} \exp\left(-\frac{h\nu_{ul}}{kT_\mathrm{ex}}\right), \tag{1.18}$$

where T_ex is the temperature that describes the excitation of the transition. In general, the temperatures describing the relative populations of different states are not the same for all transitions of a system. In fact, if the population of the upper level, n_u, is higher than that of the lower level, n_l, by more than a factor g_u/g_l, the excitation temperature of that transition will be negative. If such population inversion is achieved, the transition can give rise to amplification of radiation from a background source (or from spontaneous emission in the line itself) through the phenomenon known as microwave amplification by stimulated emission of radiation (maser).

1.3 Radiative transfer

The excitation of molecules discussed in the previous section is dependent on the physical conditions of the surrounding medium. To relate the molecular excitation to these surroundings, the transfer of radiation has to be accounted for. Here we will therefore outline the basics of radiative transfer and then give a brief description of some numerical methods that are used to solve radiative transfer problems.

1.3.1 The equations of radiative transfer

A fundamental quantity when dealing with radiative transfer is the specific intensity, I_ν ($\mathrm{J\,s^{-1}\,m^{-2}\,Hz^{-1}\,sr^{-1}}$), as this is conserved along a ray through free

space. When traveling through a medium (Fig. 1.3) it can however change if radiation is absorbed or emitted, this can be described by the equation of transfer:

$$\frac{\mathrm{d}I_\nu}{\mathrm{d}s} = -\alpha_\nu I_\nu + j_\nu, \tag{1.19}$$

where α_ν is the absorption coefficient and j_ν is the emission coefficient of the medium. For emission and absorption through transitions in molecules, the coefficients can be written in terms of the Einstein coefficients and level populations as

$$\alpha_\nu = \frac{h\nu}{4\pi}(n_l B_{lu} - n_u B_{ul})\phi(\nu) \tag{1.20}$$

and

$$j_\nu = \frac{h\nu}{4\pi} n_u A_{ul}\phi(\nu), \tag{1.21}$$

where $\phi(\nu)$ is the line profile which is not necessarily the same for α_ν and j_ν. If we now introduce the optical depth:

$$\mathrm{d}\tau_\nu = \alpha_\nu \mathrm{d}s \tag{1.22}$$

and a source function:

$$S_\nu = \frac{j_\nu}{\alpha_\nu} = \frac{n_u A_{ul}}{n_l B_{lu} - n_u B_{ul}}, \tag{1.23}$$

the transfer equation (1.19) can be rewritten as

$$\frac{\mathrm{d}I_\nu}{\mathrm{d}\tau_\nu} = -I_\nu + S_\nu. \tag{1.24}$$

Using the integrating factor e^τ we find that the solution to this equation is

$$I_\nu(\tau_\nu) = I_\nu(0)e^{-\tau_\nu} + \int_0^{\tau_\nu} S_\nu(\tau')e^{-(\tau_\nu - \tau')}\mathrm{d}\tau'. \tag{1.25}$$

Assuming a constant source function S_ν this can be further simplified to

$$I_\nu(\tau_\nu) = I_\nu(0)e^{-\tau_\nu} + S_\nu(1 - e^{-\tau_\nu}). \tag{1.26}$$

An easy interpretation of S_ν in Eq. (1.23) is possible if we rewrite it using the definition of the excitation temperature in Eq. (1.18) together with Eqs. (1.11) and (1.12)

$$S_\nu = \frac{2h\nu^3}{c^2}\frac{1}{\exp\left(\frac{h\nu}{kT_{\mathrm{ex}}}\right) - 1}. \tag{1.27}$$

This is just the expression for the radiation field from a black body at temperature T_{ex}. Equation (1.26) for the radiative transfer in a homogeneous medium can now be written as

$$I_\nu(\tau_\nu) = I_{\nu,\mathrm{bg}}e^{-\tau_\nu} + B_\nu(T_{\mathrm{ex}})(1 - e^{-\tau_\nu}), \tag{1.28}$$

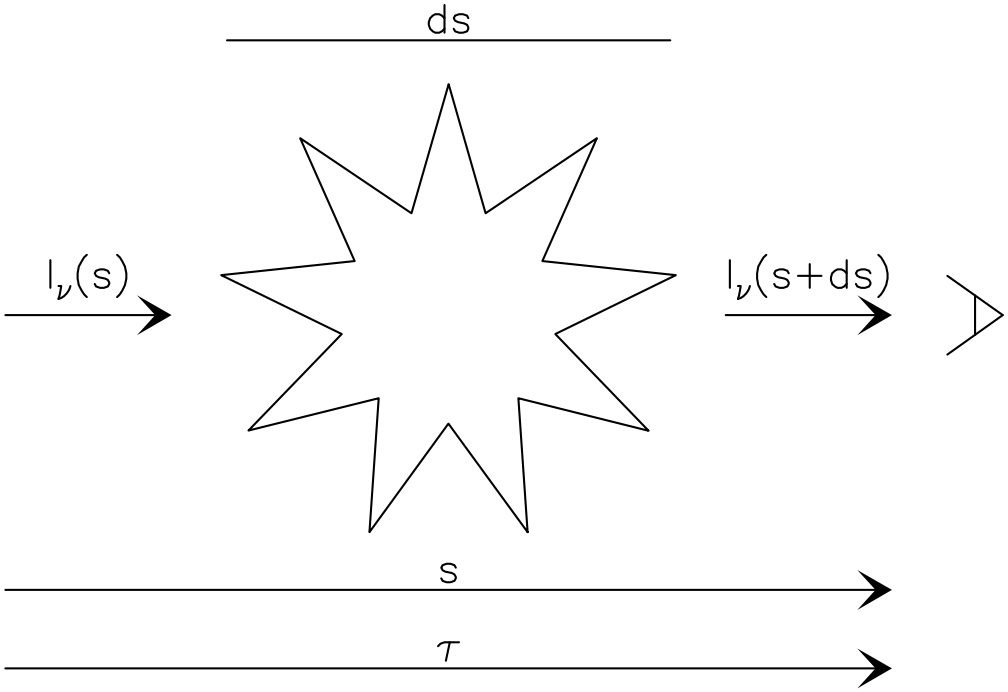

Figure 1.3: Simple sketch of the propagation of radiation through a parcel of gas, showing some of the quantities used in Eqs. 1.19-1.28 change.

where $I_{\nu,\mathrm{bg}}$ is the intensity of the background radiation.

Now that we have the solution to the transfer equation, all we have to do to get the resulting radiation field is to plug in the necessary numbers in Eq. (1.25). Unfortunately both the source function S_ν and the optical depth τ_ν depend on the level populations. To find these, we can write down the equations for statistical equilibrium as we did in Eq. (1.13). The problem is that we have to know the radiation field in order to solve these equations, as the transfer equation and the statistical equilibrium equations are coupled. There are some special cases when this problem disappears, for example in thermal equilibrium when the populations are given by Eq. (1.17), but in general it has to be solved by using iterative numerical methods. Another complication, that such methods sometimes must take into account, is the possibility of line overlaps; when two or more transitions are close in frequency, line broadening might cause the line profiles to overlap so that they affect each other in the radiative transfer analysis. The overlap could thus play an important role in the radiative pumping of levels, as has been seen in HCN where overlaps of the hyperfine components have to be considered in order to explain the ratios of the hyperfine lines (e.g., Guilloteau & Baudry, 1981; Gonzalez-Alfonso & Cernicharo, 1993). Another example where line overlaps can be important is OH, where the spin-orbit cou-

pling, Λ-doubling, and hyperfine splitting lead to a complex set of lines where some are only a couple of MHz apart in frequency.

1.3.2 Numerical radiative transfer methods

The simplest numerical radiative transfer models adopt a local approximation where photons emitted at a given position can only interact with nearby molecules. One of the most widely used local methods is the escape probability method introduced by Sobolev (1960) in the case of an expanding envelope. In this method, a factor β, known as the escape probability, accounts for the probability that an emitted photon will escape the medium. Ignoring background radiation, $\bar{J}_{ij}$ in the equations for statistical equilibrium (Eq. 1.13) now takes the form

$$\bar{J}_{ij} = S_{ij}(1-\beta), \tag{1.29}$$

where S_{ij} is the source function averaged over the line profile. Background radiation can be included by adding a term representing the background intensity multiplied with the average probability that a background photon is able to penetrate into the source. This expression can then be used to simplify the equations for statistical equilibrium (Eq. 1.13):

$$\begin{aligned}\frac{\mathrm{d}n_i}{\mathrm{d}t} =& \sum_{j<i}^{N}[-\beta n_i A_{ij}] + \sum_{j>i}^{N}[\beta n_j A_{ji}] \\ &+ \sum_{j\neq i}^{N}[n_j C_{ji} - n_i C_{ij}] + F_i - n_i D_i = 0.\end{aligned} \tag{1.30}$$

The radiation field and the level populations are now decoupled and can be solved for separately. The only remaining difficulty is to find an expression for β that depends on the optical depth but not on the radiation field. Over the years, such expressions have been developed for a number of specific geometries.

The drawback with local methods is that they are not able to handle non-local effects where radiation generated at one position in the cloud affects the populations at another position. For example, with the inclusion of radiation from dust grains mixed with the molecules, one can get an effect where the populations become thermalized at T_{dust} deep into the source where the radiation field becomes isotropic due to the surrounding dust. To deal with non-local effects, methods that solve for the radiation field at every position in the cloud are used. In theory, one such method could be to linearize the problem and solve a matrix equation involving all positions and level populations. In practice, this is far too computationally expensive and the system is instead solved by iteratively solving the equations involved. The most straightforward method to do

this is the lambda iteration method where the level populations and the intensities are calculated iteratively until the system has converged. The name of the method comes from the fact that the $\bar{J_{ij}}$ in Eq. 1.13 are expressed as a lambda operator Λ_{ij} operating on the source function S_{ij}:

$$\bar{J_{ij}} = \Lambda_{ij}[S_{ij}] = \frac{1}{4\pi} \int \Lambda_{\nu,\vec{n}}[S_\nu(\vec{x})]\phi_{ij}(\nu, \vec{n}, \vec{x}) \mathrm{d}\Omega \mathrm{d}\nu, \tag{1.31}$$

where $\Lambda_{\nu,\vec{n}}$ is the angle-dependent lambda operator, which for a given source function $S_\nu(\vec{x})$ gives the intensity $I_\nu(\vec{n})$. If we now divide the cloud into N discrete points, $\Lambda_{\nu,\vec{n}}$ can be represented by a $N \times N$ matrix, where the diagonal elements give the local contribution to the intensity in every point, while the off-diagonal elements give the non-local contributions. After assuming some initial populations, the problem is then solved by an iterative process where $\bar{J_{ij}}$ is computed for the old populations and then inserted in Eq. 1.13 to get the new populations until the solution converges. The problem with regular lambda iteration is that it converges very slowly for high optical depths. Many radiative transfer codes therefore use techniques to speed up the convergence.

In the Monte Carlo method (see e.g., Bernes, 1979, for a detailed description), all line photons emitted in the cloud during one second are simulated with a set of model photons, each representing a large number of real photons. These model photons are emitted in random directions at random locations and followed through the cloud until they either escape the medium or their weights, modified by absorption and emission events, become negligibly small. During this process, the number of absorption events in each cell of the cloud are tracked and used to calculate the new populations before a new set of model photons are released. This process is repeated until the level populations stabilize.

Another widely used method is the accelerated (or approximated) lambda iteration method (see e.g., Rybicki & Hummer, 1991, for a detailed description). It is similar to the regular lambda iteration method, with the difference that it handles high optical depths separately through a splitting of the lambda operator:

$$\Lambda_{ij} = \Lambda^*_{ij} + (\Lambda_{ij} - \Lambda^*_{ij}), \tag{1.32}$$

where Λ^*_{ij} is the approximate lambda operator which should be chosen so that it is easily inverted. The approximate lambda operator is then used to solve part of the problem using matrix inversion, while the rest of the problem is solved by regular iteration. The radiative transfer code used in papers I-III of this thesis uses accelerated lambda iteration for molecules that lack line overlaps and normal lambda iteration for molecules with line overlaps.

Chapter 2

Compact obscured nuclei

Some galaxies have significantly higher luminosities emerging from their interiors than others. This chapter deals with a subclass of such galaxies in which a large fraction of the luminosity comes from compact obscured nuclei (CONs) in their centers. As the total luminosity and spectral energy distribution of a galaxy is generally the result of a combination of different processes, determining the nature of the dominant power source in CONs is often complicated. However, active galactic nuclei (AGN) and powerful starbursts are the only known phenomena that are able to supply enough energy in a small volume; these are discussed in Sects. 2.1 and 2.2, respectively. In Sect. 2.3 we then discuss the hosts of CONs, a group of galaxies known as (ultra) luminous infrared galaxies ((U)LIRGs) and classified solely based on their total luminosity at infrared wavelengths. Finally, we turn to the CONs themselves in Sect. 2.4.

2.1 Active galactic nuclei

General references: Peterson (1997); Courvoisier (2013)

There is no formal definition of AGN, but in general the term is used for energetic phenomena, not directly related to nuclear processes in stars, in the central regions of galaxies. It is possible that all galaxies contain some kind of active nucleus, but to be recognized as an AGN the activity must contribute a substantial amount of energy over at least some portion of the electromagnetic spectrum. Since the first classification of active nuclei by Seyfert (1943), several subclasses of AGN have been identified. Early discoveries were made independently in the optical and in radio and it was not clear from the beginning that the objects were of the same underlying nature. A review of the history of AGN from the beginning of the 20th century until the 1980s is given by Shields (1999).

The variability on timescales from months down to minutes in some of the objects constrains the size of the emitting region to scales considerably smaller than 1 pc. The extreme luminosities, sometimes outshining entire galaxies, emerging from these tiny regions led to the conclusion that the nature of the power source must be gravitational, as nuclear processes are simply not efficient enough. The current understanding is that the origin of the power is accretion of matter onto a supermassive black hole (SMBH). With this in mind, the mass of the compact object can be estimated using the Eddington luminosity, the luminosity above which the outward force due to radiation pressure from a radiating object exceeds the gravitational attraction of the object. If the radiation pressure is acting on pure ionized hydrogen the Eddington luminosity is given by

$$L_{\rm Edd} = \frac{4\pi GMc}{\kappa} \simeq 3.2 \times 10^4 \left(\frac{M}{M_\odot}\right) L_\odot, \tag{2.1}$$

where $\kappa = \sigma_{\rm T}/m_{\rm p} \approx 0.4$ cm^2 g^{-1} is the opacity of the ionized gas, $m_{\rm p}$ is the mass of the proton and $\sigma_{\rm T}$ is the Thomson scattering cross-section of the electron. This limit will change if the radiation pressure is mainly acting on material with a different opacity, and in a dust enshrouded AGN the effective Eddington limit can be significantly lower (e.g., Fabian et al., 2006). Since the brightest observed AGN have luminosities above 10^{13} L$_\odot$ (Türler et al., 1999), the implied mass of the compact object can be as high as 10^9 M$_\odot$. Of course, in order for this to work as a power source, there has to be an ample supply of material close to the nucleus as well as a process in which this material can lose angular momentum and be accreted onto the SMBH.

The different subclasses of AGN are very heterogeneous in their observed characteristics, but in general they have high luminosities and a relatively flat continuum in νF_ν from X-rays to the far infrared, with a steep decline between 100 μm and radio wavelengths. Other observable characteristics of different types of AGN include narrow ($\lesssim 1000$ km s^{-1}) permitted and forbidden emission lines in both Type 1 and Type 2 AGN, broad ($\lesssim 10,000$ km s^{-1}) permitted emission lines in Type 1 AGN, radio jets in some radio galaxies, and rapid variability and high polarization in blazars. A summary of the largest subclasses and their properties can be found in Table 2.1.

Efforts have been made to explain this observed diversity with a single kind of object observed under different conditions. The most popular of such unified models today are those where the apparent differences arise due to different viewing angles toward an object similar to the one schematically shown in Fig. 2.1 (see e.g., Antonucci, 1993; Urry & Padovani, 1995). In the simplest case, the difference between a Seyfert 1 and a Seyfert 2 is that the former is viewed almost face-on, so that both the broad line region (BLR) and the narrow line region (NLR) are visible, while the latter is viewed edge-on, so that the BLR is hidden by the molecular torus.

Table 2.1: Subclasses of AGN

Class	Broad lines	Narrow Lines	Radio loudness
Seyfert 1	Yes	Yes	Radio quiet
Seyfert 2	No	Yes	Radio quiet
Broad line radio galaxies	Yes	Yes	Radio loud
Narrow line radio galaxies	No	Yes	Radio loud
Quasi-stellar objects	Yes	Yes	Radio quiet
Quasars	Yes	Yes	Radio loud
Blazars	No	No	Radio loud

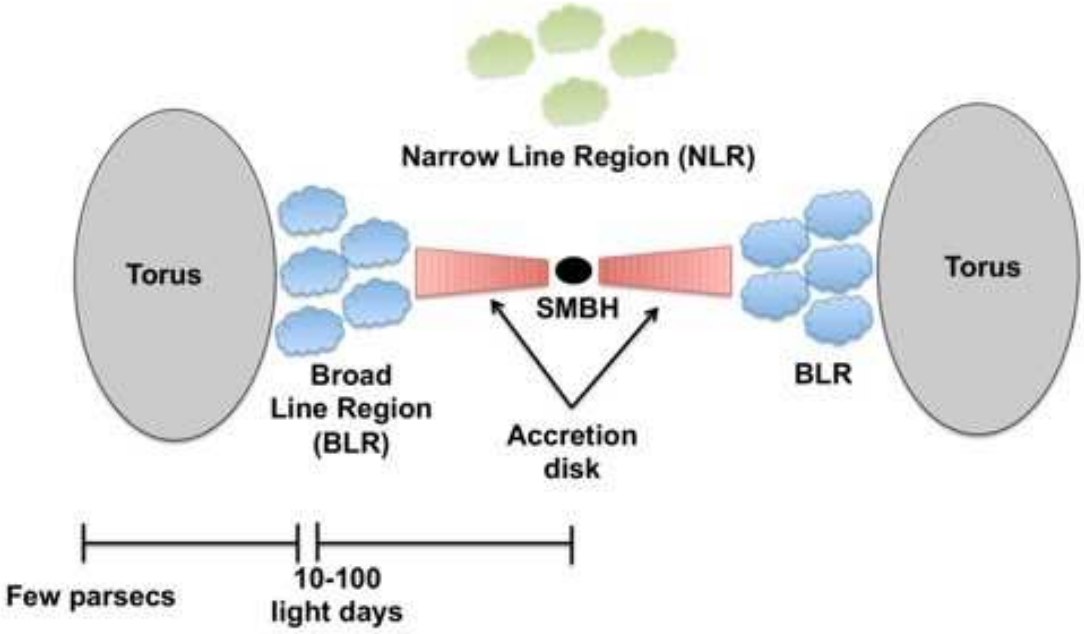

Figure 2.1: Schematic view of the structure of an AGN in the unification models. The class of AGN seen depends on the viewing angle with respect to the torus. Credit: Claudio Ricci - `http://www.isdc.unige.ch/~ricci/Website/Active_Galactic_Nuclei.html`

2.2 Starburst galaxies

General references: Moorwood (1996)

Some galaxies show signs of recent star formation activity at a rate significantly higher than in normal galaxies, these are generally referred to as starburst galaxies. The star formation rate (SFR) in these objects is so high, $3 - 30\ \mathrm{M}_{\odot}\ \mathrm{yr}^{-1}$ in

medium luminosity starbursts, that they would consume all the available gas in a short time compared to the age of the galaxy. A starburst can therefore clearly be no more than a short phase in the life of a galaxy. Typical characteristics include strong emission-line spectra from HII-regions and a prominent peak in the far infrared associated with emission from dust heated by young massive stars. The vigorous star formation is sometimes located in regions outside the nucleus of the galaxy (e.g., the Antennae; Neff & Ulvestad, 2000) but most of the time it is confined to a region in the central kpc; within the context of this thesis we are mainly concerned with these nuclear starbursts.

Although not as compact as AGN, nuclear starbursts also require a process that can transport large amounts of gas to the central regions of the host galaxy and fuel the activity. In order to do this, the gas must lose most of its angular momentum. This can be accomplished by torques created by non-axisymmetric perturbations of the gravitational potential, such as those induced by stellar bars (e.g. Schwarz, 1984; Noguchi, 1988; Shlosman et al., 1989) or interactions with other galaxies (e.g. Mihos & Hernquist, 1996). Based on IRAS observations, Sanders et al. (1986) suggested that the most spectacular starbursts are produced in galaxy mergers. Hybrid N-body/gas dynamics simulations performed by Barnes & Hernquist (1991) showed that the merging of two galaxies can indeed assemble large amounts of gas in the nucleus of the resulting new galaxy.

As for AGN, there are limits to the luminosity of starbursts. In their observations of starbursts around nine Seyfert nuclei, Davies et al. (2007) found surface brightnesses approaching 10^{13} $L_\odot$ kpc^{-2} in the central parsecs. These observations can be explained by an Eddington-like limit based on a model in which the gas disk is supported by stellar radiation pressure (Thompson et al., 2005). As long as the dust temperature is below 200 K, the limit is $\sim 10^{13}$ $L_\odot$ kpc^{-2}, independent of the temperature. Expressed in luminosity per unit mass this limit becomes $500 - 1000$ $L_\odot$ $M_\odot^{-1}$ (Scoville, 2003; Thompson et al., 2005). The reason for the temperature-independence of the surface brightness is the fact that the Rosseland mean opacity is proportional to $T_{\rm dust}^2$ for $T_{\rm dust} < 200$ K, canceling a similar factor in the expression for the surface brightness. For starbursts with dust temperatures between 200 K and the dust sublimation temperature ($\sim$1500 K), the opacity is roughly constant, and the surface brightness may increase by two orders of magnitude to $\sim 10^{15}$ $L_\odot$ kpc^{-2}, depending on the temperature (Andrews & Thompson, 2011).

2.3 (Ultra) Luminous infrared galaxies

General references: Sanders & Mirabel (1996); Lonsdale et al. (2006)

The far-infrared all-sky survey performed with the Infrared Astronomical Satellite (IRAS) in 1983 resulted in the detection of tens of thousands of galaxies, many of which emit most of their energy in the infrared. Although the existence of galaxies with high infrared luminosities was known before IRAS, this was the first time that they where discovered in large numbers. Now we know that these infrared galaxies constitute the majority of the most luminous galaxies, those with bolometric luminosities above 10^{11} $L_{\odot}$, in the local Universe (Sanders & Mirabel, 1996). Two specific classes of galaxies are often mentioned, the luminous infrared galaxies (LIRGs) with luminosities of $10^{11} - 10^{12}$ $L_{\odot}$ in the $8 - 1000$ μm range, and the ultraluminous infrared galaxies (ULIRGs) with luminosities above 10^{12} $L_{\odot}$ in the same wavelength range. At high luminosities these objects constitute the dominant population, but in the local Universe they are still relatively rare compared to less luminous objects, as can be seen from the luminosity function in the left panel of Fig. 2.2. Although (U)LIRGs are rare in the local Universe, surveys at millimeter and submillimeter wavelengths (e.g. Smail et al., 1997; Hughes et al., 1998) have shown that they are much more numerous at redshifts above unity. It is thus likely that they have had an important role to play in the formation and evolution of galaxies in the early Universe.

The right panel of Fig. 2.2 shows the mean spectral energy distribution (SED) from submillimeter to UV wavelengths for infrared galaxies of different luminosities. The SED of a typical (U)LIRGs is dominated by a strong starburst-like peak around 60 μm due to warm dust emission, a systematic shift in this peak towards shorter wavelengths, indicating an increase of the average $T_{\rm dust}$, can be seen with increasing luminosity. If the galaxy contains an AGN, and the mid-IR dust emission is not fully extincted by colder surrounding dust, an additional peak can be seen closer to 25 μm due to dust heated directly by the active nucleus. In addition there is a peak in the optical associated with thermal radiation from stars. Note that the optical peak only changes by a factor of about three when the far-infrared emission increase by three orders of magnitude.

The extreme infrared luminosities of (U)LIRGs imply the existence of an energetic power source, heating the large columns of warm dust that is responsible for the bulk of the observed radiation. Due to these large columns of obscuring material the nature of the power source is often unclear, but the large energy densities involved suggest a compact starburst or an AGN. The most luminous objects all seem to be the results of strong interactions or mergers where copious amounts of gas are funneled into the nucleus, available to feed a nuclear starburst, an AGN, or both. Based on this information, an evolutionary scenario

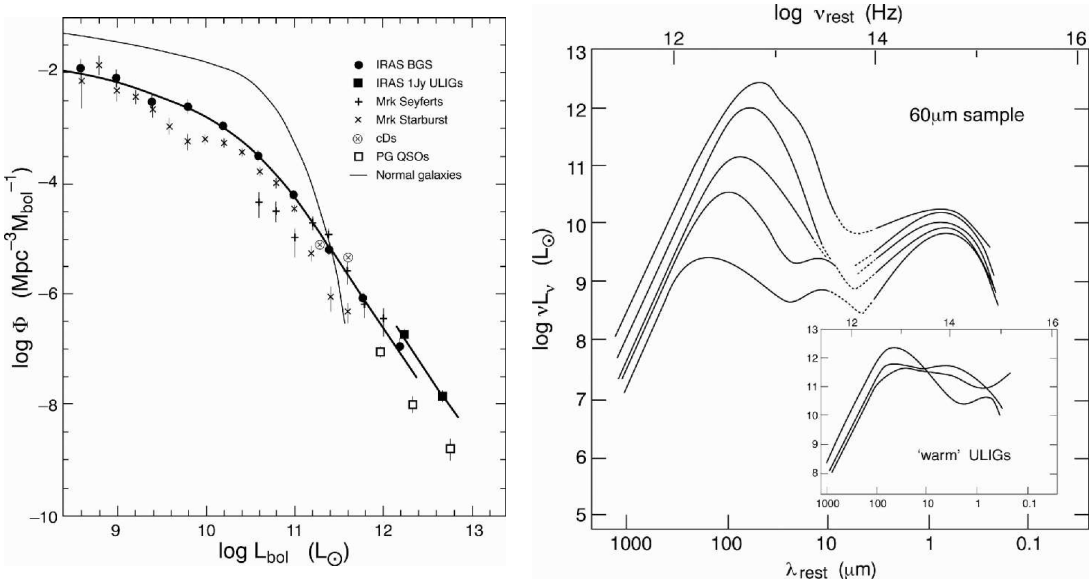

Figure 2.2: *Left:* Luminosity function of local infrared galaxies compared with those of other classes of galaxies. *Right:* Mean spectral energy distributions for a sample of 60 μm-selected infrared galaxies from submillimeter to UV wavelengths. The different curves show how the SEDs vary as $L_{\rm IR}$ increases (from the bottom up). Both figures are from Sanders & Mirabel (1996).

has been suggested by Sanders et al. (1988) in which the merging of two galaxies leads to a ULIRG dominated by a nuclear starburst. This starburst phase is then followed by the ignition/feeding of an AGN which heats the surrounding dust to produce a warmer ULIRG, before feedback from the AGN eventually clears the dust to reveal a quasar in the optical, UV and X-ray. Based on interferometric radio observations, Condon et al. (1991) concluded that many of the brightest IRAS galaxies are powered by nuclear starbursts so compact that they are optically thick to free-free radiation at 1.49 GHz. The Compton-thick nature of such objects would also render even hard (2-10 keV) X-rays unable to penetrate the obscuring material.

Due to the large columns obscuring the nuclei of (U)LIRGs at many wavelengths, alternative probes of the nuclear activity are needed. One widely used diagnostic tool available in some (U)LIRGs are the OH megamasers in which the main lines of the ground state Λ-doublet of OH exhibit strong masing. These are located in the dense molecular gas in the nuclei of some (U)LIRGs and have luminosities a million times higher than those of the strongest Galactic OH masers. The 18 cm OH megamasers lines can for example be used to detect nuclear outflows in otherwise obscured galaxies (Baan et al., 1989). In the next chapter of this thesis, and in Papers I-III, we investigate the ability of H_2O and OH to probe the far-infrared radiation field to learn more about the physical

conditions in obscured nuclei. In Paper IV, we also attempt to use non-masing transitions within the two first rotationally excited states of OH to detect outflowing gas in an OH megamaser galaxy.

2.3.1 Molecular outflows

Outflows driven by AGN or starburst activity constitute an effective feedback mechanism that is able to clear large amounts of dust and molecular gas from the nuclear regions and stop the growth of both the SMBH and the stellar component. This kind of self-regulation has been invoked (e.g., by Fabian, 1999; Murray et al., 2005; Hopkins et al., 2009) to explain the tight correlation seen between the masses of supermassive black holes and host galaxy properties such as the velocity dispersion or the bulge mass (e.g., Magorrian et al., 1998; Ferrarese & Merritt, 2000). In addition, AGN feedback has an important role to play in evolutionary scenarios that start with a galaxy merger and end with the clearing of dust and gas surrounding the SMBH (e.g., Sanders et al., 1988).

Although the molecular component of such outflows may carry a significant fraction of the mass and momentum, few examples of molecular outflows (e.g., Turner, 1985; Nakai et al., 1987; Baan et al., 1989; Walter et al., 2002; Sakamoto et al., 2009) had been observed until fairly recently. With the advent of *Herschel*, massive molecular outflows traced by far-infrared OH lines were quickly discovered (e.g., Fischer et al., 2010; Sturm et al., 2011). In a systematic search for molecular outflows traced by OH in luminous galaxy mergers, Veilleux et al. (2013) found that faster outflows tend to be associated with more luminous AGN, suggesting that the AGN plays a role in driving outflows. In addition, they found that the most AGN dominated systems often exhibit modest outflow velocities, something that they interpret as possible evidence that AGN feedback declines once a path has been cleared through the surrounding dusty material. More recently, González-Alfonso et al. (2017) analyzed the energetics of molecular outflows in local ULIRGs detected in OH with *Herschel* and found that, overall, the outflows are momentum driven by a combination of AGN and starburst activity. However, in a fifth of the sources they found that the outflows seem to be driven by powerful AGN feedback, uncorrelated with the merging phase and possibly representing stochastic strong feedback events occuring throughout the merging process. Another powerful method to study molecular outflows is offered by (sub)millimeter interferometers that allow for mapping of the molecular emission (e.g., Feruglio et al., 2010; Aalto et al., 2012; García-Burillo et al., 2014, 2015; Pereira-Santaella et al., 2016). In an interferometric study of CO $J = 1 - 0$ in local ULIRGs and AGN hosts, Cicone et al. (2014) found that, although starbursts are able to drive massive molecular outflows, the presence of an AGN is able to significantly strengthen the outflow and thus quench the star formation.

2.4 Compact obscured nuclei

An emerging new subclass of galaxies are the compact obscured nuclei found in some (U)LIRGs. In their observations of the LIRG NGC 4418, Costagliola & Aalto (2010) found unusually bright lines of vibrationally excited HC_3N, which they argue are excited by a very compact (a few pc) mid-infrared source with high surface brightness. Subsequent surveys (Costagliola et al., 2011; Lindberg et al., 2011) showed that unusually luminous HC_3N emission is seen in a small fraction of (U)LIRGs, again suggesting the presence of compact dusty nuclei with high surface brightnesses. Indeed, high resolution mm and submm studies (e.g. Sakamoto et al., 2008, 2010, 2013; Costagliola et al., 2013; Aalto et al., 2015) have revealed that some of these galaxies host compact, opaque dust sources where a large fraction of the luminosity of the galaxy emerges from regions within 100 pc of the nucleus. The nuclear activity in these objects is hidden behind large columns ($N_{\rm H_2} > 10^{24}$ cm^{-2}) of molecular gas and warm ($T > 100$ K) dust. The intense IR fields and shielded environments give rise to very rich molecular spectra. A good example is the central regions of the LIRG NGC 4418 where vibrational temperatures of $200 - 400$ K in HCN, HNC, and HC_3N are found within a core of radius less than 5 pc (Aalto et al., 2007; Costagliola & Aalto, 2010; Sakamoto et al., 2010; Costagliola et al., 2013). Another notable example is the LIRG Zw 049.057 (Papers I and IV) whose submm spectrum is shown in Fig. 2.3. A list of the currently known local CONs and some of their properties is included in Table 2.2.

The high level of obscuration in CONs poses a problem for the study of the nuclear regions; Aalto et al. (2015) found evidence that traditional dense-gas tracers such as the rotational lines in the vibrational ground states of HCN and HCO^+ are heavily affected by self- and continuum absorption, and cannot be used to probe the inner regions of CONs. They suggest that the nuclear environments are better traced by rotational lines of vibrationally excited ($v_2 = 1$) HCN, which have been detected in all CONs where they have been observed (Sakamoto et al., 2010; Aalto et al., 2015). All CONs also have large columns of warm dust (e.g. González-Alfonso et al., 2012; Falstad et al., 2015, 2017) which is heated when the radiation from the central energy source is absorbed by the surrounding dust and then re-emitted at progressively longer wavelengths as it diffuses outwards (González-Alfonso et al., 2012). This creates an ideal environment for various molecular species, very similar to the one in hot molecular cores around young massive stars (Rolffs et al., 2011). In addition, in their line survey, Costagliola et al. (2011) found that all sources with detectable HC_3N also have above average HNC/HCN ratios and HCO^+/HCN < 1, consistent with the hot core models of Bayet et al. (2008). The intense IR field and abundance of molecular gas also provide the necessary conditions for OH megamaser activity; the only CON not listed as an OH megamaser in the sample of (Henkel

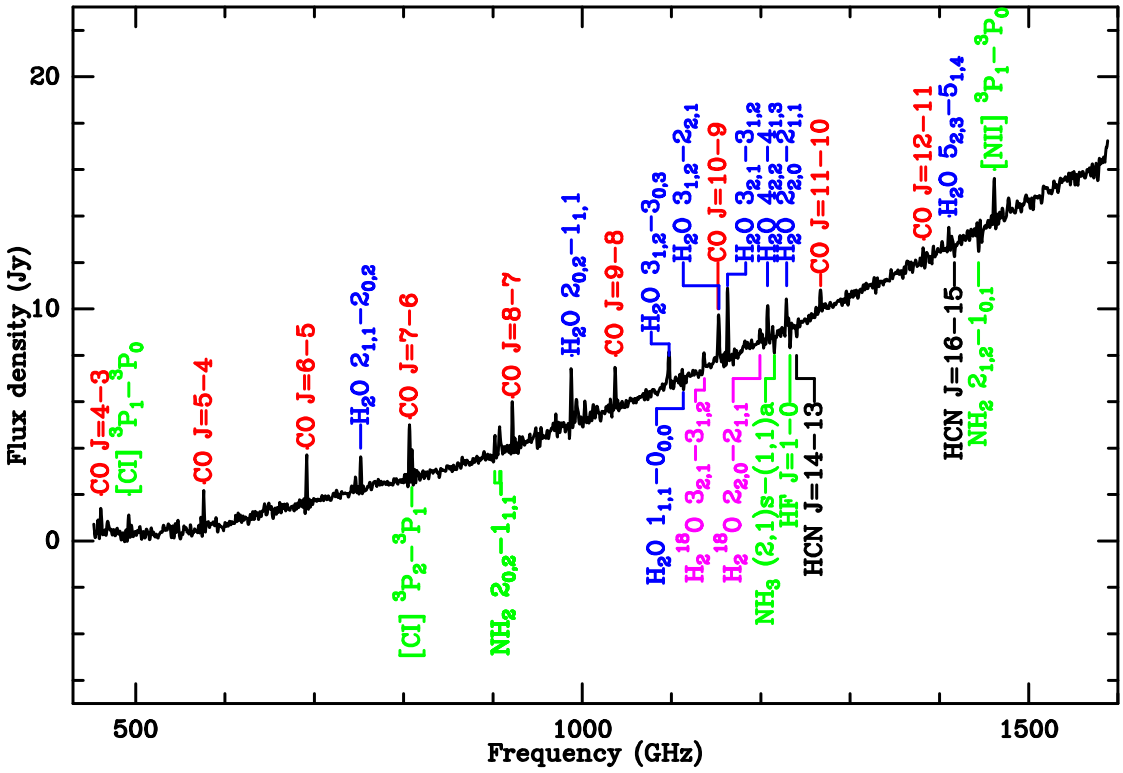

Figure 2.3: Submillimeter spectrum of Zw 049.057 taken with the SPIRE instrument onboard *Herschel* and discussed in Paper I.

& Wilson, 1990) is IC 860, which instead is listed as a lower luminosity kilomaser. More puzzling is the enhancement of ^{18}O with respect to ^{16}O which is seen in some CONs (Martín et al., 2011; González-Alfonso et al., 2012, e.g. Arp 220;), but not in others (González-Alfonso et al., 2012, e.g. NGC 4418;). Similarly, the presence of in- or outflowing gas also seems to vary between different sources, with molecular outflows detected in three quarters of the CONs (see Table 2.2) using the OH far-IR (e.g. Veilleux et al., 2013) or megamaser lines (Baan et al., 1989). In the case of Arp 220 and NGC 4418, González-Alfonso et al. (2012) tentatively attributed these differences to evolutionary effects. According to their reasoning, the higher ^{16}O/^{18}O ratio in NGC 4418 indicates a young starburst component, since the ratio is expected to decrease with new star forming generations as ^{16}O is a primary isotope which can be produced by stars initially consisting of only hydrogen, while ^{18}O is a secondary one whose formation requires the existence of heavier elements from previous stellar generations (Prantzos et al., 1996). This is consistent with the presence of an inflow and lack of a molecular outflow, which also indicate that NGC 4418 is experiencing an earlier evolutionary phase, before the onset of mechanical feedback

Table 2.2: Known compact obscured nuclei

Source	Class	OH megamaser	^{18}O enh.	HCN-vib	Mol. outflow
NGC 4418	LIRG	Yes[1]	No[2]	Yes[3]	...
IC 860	LIRG	No[1]	...	Yes[4]	...
Zw 049.057	LIRG	Yes[1]	Yes[5]	Yes[4]	Yes[5,6]
Arp 299A	LIRG	Yes[1]	No[7]	...	Yes[8]
Arp 220	ULIRG	Yes[1]	Yes[2]	Yes[4]	Yes[2,8]
IRAS 17208-0014	ULIRG	Yes[1]	...	Yes[4]	Yes[9]
IRAS 11506-3851	LIRG	Yes[1]	...	...	Yes[10]
UGC 5101	ULIRG	Yes[1]	...	Yes[11]	Yes[11]

[1] Henkel & Wilson (1990) [2] González-Alfonso et al. (2012) [3] Sakamoto et al. (2010)
[4] Aalto et al. (2015) [5] Paper I [6] Paper IV [7] Paper II [8] Baan et al. (1989)
[9] Veilleux et al. (2013) [10] Pereira-Santaella et al. (2016) [11] König et al. in prep.

(González-Alfonso et al., 2012). In contrast, the lower ^{16}O/^{18}O ratio and the presence of outflowing molecular gas (Baan et al., 1989) in Arp 220 places it in a more advanced phase of its activity.

The hot core-like properties of CONs suggest that these dust covered objects might represent the early stages of nuclear activity. If they are indeed in an early evolutionary phase, they might be the ideal laboratories to study the final phase of inflow and the onset of outflows. The properties of the in- and outflowing gas would then be important in order to understand the nuclear activity and it is possible that they can provide important clues about the evolution of active galaxies. Furthermore, the high luminosities emerging from these compact regions indicate that the hidden power source must be an AGN, a nuclear starburst, or both. A good example is Arp 299A where evidence of a low-luminosity AGN (Pérez-Torres et al., 2010) has been found in a region already known to have hosted a recent starburst (Pérez-Torres et al., 2009). There are several reasons for trying to determine if it is an accreting black hole, a compact starburst, or a combination of the two that provide the CONs with their energy. For example, obscured star formation is linked to the assembly of stellar mass in massive galaxies (Ibar et al., 2013) and it is possible that more than 50% of the star formation at high redshift was obscured (e.g. Chapman et al., 2005; Wardlow et al., 2011). It is also commonly accepted that obscured AGN are needed in order to explain the spectral shape of the cosmic X-ray background (e.g. Comastri et al., 1995; Gilli et al., 2007) and it has been found that as much as $20 - 30\%$ of the AGN might be Compton-thick (e.g. Burlon et al., 2011), a situation that is likely even more common in low-luminosity AGN (e.g. Lusso et al., 2013; Merloni et al., 2014). The possibility that CONs harbor completely obscured AGN is also interesting in view of the model suggested by Fabian et al. (1998) in which low-luminosity AGN can be completely obscured by nuclear (within

the inner 100 pc) starbursts. On the observational side, Ueda et al. (2007) suggested that there are a significant number of obscured AGN with very high covering factors of the obscuring material in the local Universe. For high redshift sources, Brightman & Ueda (2012) used X-ray spectral fitting with models that account for the geometry of the surrounding material and found evidence that 20% of AGN in the *Chandra* Deep Field South might be completely buried, with a covering factor of almost 100%. According to Elitzur (2012), the variation of the torus covering factor among AGN has great implications for unification schemes, and it is essential to determine its intrinsic distribution function to be able to do meaningful studies of unification statistics. Regardless of the exact nature of the hidden power source, we are likely witnessing a phase of fast nuclear mass growth in the form of accretion onto a supermassive black hole, the build-up of a nuclear stellar component, or both. The study of CONs might thus be essential for our understanding of nuclear growth and the feedback processes associated with it. Finally, in addition to the things we can learn about the nature and evolution of active galaxies, CONs also constitute interesting objects themselves. The unique physical conditions prevailing in obscured nuclei provide us with the opportunity to study molecular chemistry and excitation in extreme environments where intense IR fields often dominate the excitation (e.g., González-Alfonso et al., 2012, 2013).

Chapter 3

Probing the physical conditions in compact obscured nuclei

As noted in the previous chapter, studies of compact obscured nuclei are important for our understanding of the onset and evolution of nuclear activity in galaxies. Unfortunately the obscuring material of the CONs may be opaque at most wavelengths, effectively hiding the central regions from examination using conventional methods like optical or IR lines, and in some cases even X-rays. It is therefore important to find tracers that are able to penetrate the optically thick barrier and convey information about the extreme environment close to the nucleus.

This can be accomplished by going to longer wavelengths where the obscuring dust is less optically thick. One way to do this is via space-based observations in the far-IR and submillimeter to study the obscuring dust itself. Section 3.1 contains a discussion about such observations, with a focus on the light hydrides H_2O and OH as well as radiative transfer modeling as a way to interpret the observations. It also contains a short description of the *Herschel* Space Observatory which is used in Papers I-III, as well as a brief summary of similar work that has been done in the local Universe. Another approach is to use ground based observations at even longer wavelengths to try to see through the obscuring material in order to probe the physical conditions in the nucleus. This can, for example, be accomplished by observing molecular species that are radiatively excited by the intense infrared field near the nucleus and then emit radiation at longer wavelengths where the optical depth is lower. Examples include the rotational lines of vibrationally excited molecules like HCN, HNC and HC_3N, which can be used to probe deep into the cores of CONs (e.g. Aalto, 2013; Aalto et al., 2015), but also the Λ-doublet transitions in rotationally excited OH (e.g. Henkel & Wilson, 1990). In Sect. 3.2 observations at (sub)mm and radio wavelengths are discussed, with a focus on interferometric observations. A

short description of the instruments used in Papers III and IV is also included, as well as a brief summary of other (sub)mm and radio observations of CONs.

3.1 Observations in the far infrared and submillimeter

The emission from rotational transitions of molecules generally occur at wavelengths ranging from the radio for heavy polyatomic species to the far-infrared for light hydrides like H_2O. Due to atmospheric absorption, not all of these wavelength regions are available to ground-based telescopes. This is not a big problem at radio wavelengths, but at shorter wavelengths, especially those corresponding to the absorption bands of abundant species like H_2O, a lot of the radiation is absorbed by atmospheric gases. At submillimeter wavelengths ground-based observations are still possible in certain atmospheric windows, but they generally require high and dry sites to minimize absorption by atmospheric water vapor. This is the reason for the location of, for example, the Atacama Large Millimeter/submillimeter Array (ALMA) at the Chajnantor plateau in the Atacama desert of Chile. At frequencies above ~ 1 THz (wavelengths below ~ 300 μm) most of the radiation is however absorbed by atmospheric species even at these sites. In order to do observations at these wavelengths one alternative is to use airborne observatories like the Stratospheric Observatory for Infrared Astronomy (SOFIA). To avoid the problem with absorption in the atmosphere altogether, space-based observatories like *ISO* and *Herschel* have been employed for observations from infrared to submillimeter wavelengths.

3.1.1 *Herschel* Space Observatory

The *Herschel* Space Observatory (Fig. 3.1) was a space-based observatory in the $55 - 671$ μm spectral range operating from 2009 until 2013 when it ran out of liquid helium used for cooling its instruments. With its 3.5 m Cassegrain antenna it is still the largest infrared space telescope ever launched. *Herschel* was put in an orbit around the second Lagrangian point (L2) of the Earth-Sun system, where the gravitational forces from the Earth and the Sun make it possible for an object to orbit the Sun with the same period as the Earth. On board, it carried three instruments: the Photodetector Array Camera and Spectrometer (PACS), an imaging photometer and spectrometer covering the spectral range $55 - 210$ μm; the Spectral and Photometric Imaging Receiver (SPIRE), an imaging photometer and spectrometer covering the spectral range $194 - 672$ μm; and the Heterodyne Instrument for the Far Infrared (HIFI), a heterodyne spectrometer covering the frequencies $480 - 1250$ GHz and $1410 - 1910$ GHz.

Figure 3.1: Artist's impression of the Herschel spacecraft. Credit: ESA/ AOES Medialab; background: Hubble Space Telescope image (NASA/ESA/STScI)

3.1.2 H_2O and OH as probes of the warm dust emission in CONs

In order to study the dusty cores of CONs we need a probe that is sensitive to the intense far-infrared radiation fields present in these objects. Due to their small moments of inertia, the light hydrides have large rotational constants and thus large differences in energy between their rotational levels, see Sect. 1.2.2 for the equations governing the energies of rotational levels in molecules. Because of this, they have many transitions that occur at far-infrared or submillimeter wavelengths.

The asymmetric top molecule H_2O has a multitude of rotational transitions at the wavelengths of interest, its rich spectrum spans the entire far-infrared and submillimeter portions of the electromagnetic spectrum available to PACS and SPIRE. Due to its relatively high dipole moment, the transitions of H_2O have fast radiative rates and, as long as it is not located in an extremely warm and dense environment, H_2O is an excellent probe of the underlying continuum in the far-infrared, that is, at the wavelengths where the galaxy SED peaks. With the exception of the ground-state $1_{11} \rightarrow 0_{00}$ transition, the lines with rest wavelengths in the SPIRE spectral range are almost always seen in emission. Modeling of these lines performed by González-Alfonso et al. (2014) suggests that they are pumped by the far-infrared continuum where four absorption lines at approximately 45, 58, 75, and 101 μm can account for the excitation. For the

$1_{11} \rightarrow 0_{00}$ line there exists no such pumping mechanism and the upper level can only be radiatively excited by a photon with the same frequency as the line emission. This line is therefore more sensitive to collisional excitation and thus to the density and temperature of the surrounding gas. In the right part of Fig. 3.2 the energy level diagram of H_2O is displayed with lines indicating the transitions that where detected with PACS and SPIRE in Papers I-III.

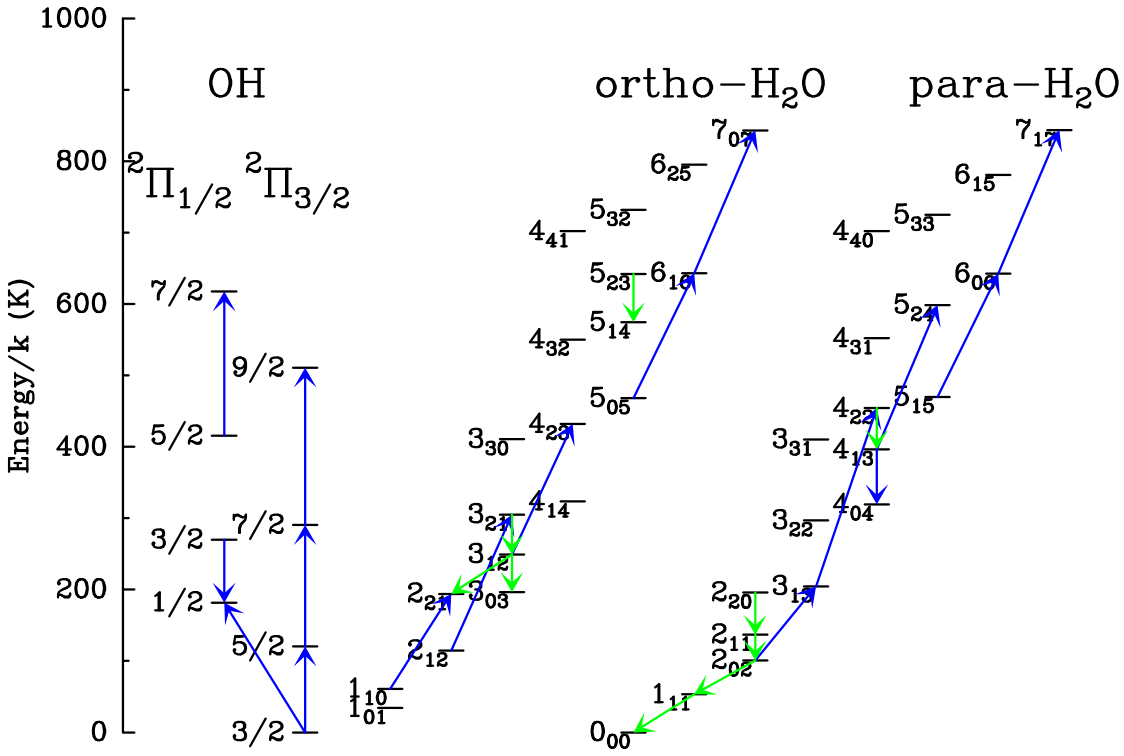

Figure 3.2: Energy level diagrams of OH and H_2O (ortho and para). Blue and green arrows indicate lines observed with PACS and SPIRE, respectively, in Papers I-III.

Just as H_2O, OH has a relatively high dipole moment and many transitions in the far infrared. Unlike H_2O, OH has a non-zero electronic angular momentum in the ground state which interacts with the rotation of the molecule to create energy-level splitting in the rotational levels, so-called Λ-doubling. Because of this, the far-infrared lines of OH come in the form of doublets as seen in Fig. 3.3. In addition, its non-zero electronic spin couples with the electronic angular momentum, giving rise to the $^2\Pi_{3/2}$ and $^2\Pi_{1/2}$ splitting seen in the energy diagram in Fig. 3.2. In regions with a strong far-infrared radiation field, the levels of OH are expected to be radiatively excited, but the ground state lines, especially the $^2\Pi_{3/2} - ^2\,\Pi_{3/2}\,\frac{5}{2} - \frac{3}{2}$ transition at approximately 119 µm, can still be affected by collisional excitation. In the left part of Fig. 3.2 the energy level diagram of OH is displayed with lines indicating the transitions that where detected with PACS

in Papers I and II. The hydroxyl molecule has also proven to be a good tracer of massive molecular outflows (e.g. Fischer et al., 2010; Sturm et al., 2011).

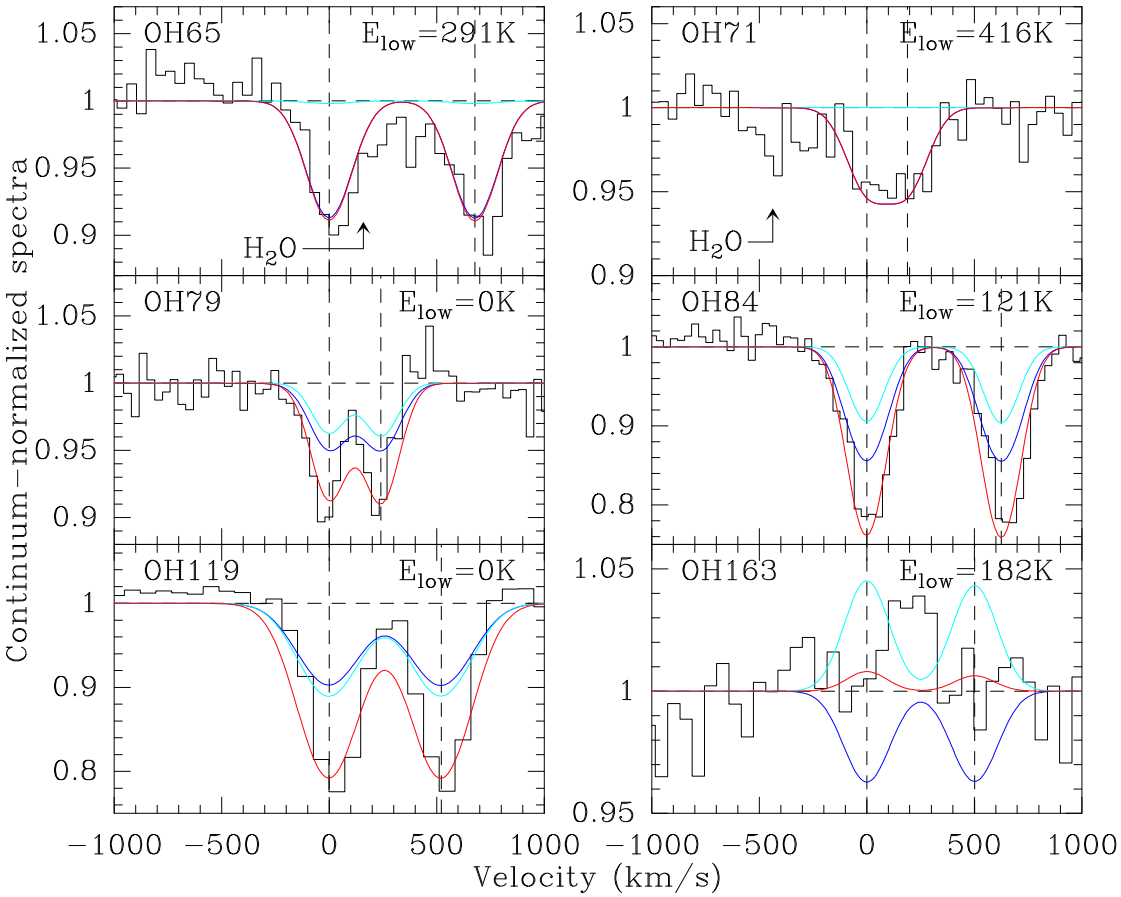

Figure 3.3: Far-infrared OH doublets observed in Zw 049.057 with PACS, the colored lines represent models from Paper I.

3.1.3 Probing dusty nuclei with space-based far-IR and submillimeter observations

With their many transitions in the far infrared, H_2O and OH are excellent probes of warm dust in the nuclear regions of (U)LIRGs. Observations and subsequent radiative transfer modeling of these species together with the dust continuum make it possible to put constraints on important properties such as the temperature and optical depth of the dust and in Papers I-III we do just this. In this section we give a short summary of previous modeling work based first on *ISO* and then *Herschel* observations. While H_2O and OH are the main molecules concerned in this thesis, some of the following authors have also used other

species in their analyses.

When *ISO* opened up the mid- and far-infrared wavelength regimes for spectroscopy, it became possible to study the dusty nuclei of (U)LIRGs in detail. Based on observations with *ISO*, Spinoglio et al. (2005) were able to model the overall continuum as well as the atomic spectrum of NGC 1068 with a combination of an AGN and a starburst. In addition, they performed an analysis of the OH lines at 79, 119, and 163 μm which were all detected in emission in this source. They concluded that, unlike the lines at 79 and 163 μm, the OH line at 119 μm cannot be radiatively excited in NGC 1068 but must originate in a region of warm and dense gas where it is collisionally excited. The results of their radiative transfer models further led them to conclude that the bulk of the OH emission arises in the nuclear region of the galaxy, possibly with small contributions from the extended starburst. Models of the ULIRGs Arp 220 and Mrk 231 by González-Alfonso et al. (2004) and González-Alfonso et al. (2008), respectively, revealed warm, optically thick nuclear regions with dust temperatures of ~ 100 K within diameters of ~ 100 pc. In both sources, the excitation of H_2O and OH could be explained by radiative excitation by the far-infrared emission from the warm dust. While both galaxies were found to have high column densities of H_2O and OH towards their nuclei, the models of Arp 220 also indicated an H_2 column of $\sim 10^{25}$ cm^{-2}, high enough to obscure a buried X-ray source.

The limits to the spectral resolution and sensitivity of *ISO* put some constraints on the ability to detect weaker lines and determine the kinematics associated with, for example, the OH detections. With the advent of *Herschel* it became possible to make observations with higher resolution and sensitivity. With these new observations at hand, Fischer et al. (2010) detected a molecular outflow in OH and ^{18}OH with velocities in excess of 1000 km s^{-1} in Mrk 231. Besides the high outflow velocities, modeling of the emission indicated an extremely low ^{16}O/^{18}O ratio of $\sim 30-40$ which they suggested may be due to advanced starburst activity. In the SPIRE spectrum of the same galaxy, González-Alfonso et al. (2010) detected seven rotational lines of H_2O with upper level energies as high as 640 K. Their radiative transfer models indicated the presence of a warm (~ 100 K) dust component with a radius of ~ 100 pc that is able to radiatively excite the high-lying lines through absorption of far-infrared photons. In addition they noted that a cooler component with a radius of ~ 600 pc is needed to fully account for the lower-lying lines. They conclude that although it gave new clues to the origin of H_2O in Mrk 231, the new analysis supports the old conclusions that where based on observations with *ISO*.

Based on full range PACS spectroscopy González-Alfonso et al. (2012) performed an analysis of the excitation in Arp 220 and the LIRG NGC 4418. They found very high excitation in H_2O, OH, HCN and NH_3 in both galaxies but overall the excitation was somewhat higher in NGC 4418 than in Arp 220. To

account for this high excitation, the radiative transfer models indicated the need for warm (> 100 K), optically thick dust components in the nuclei of both galaxies. These nuclear components both have high surface brightnesses, in excess of 10^{13} $L_\odot$ kpc^{-2}, which the authors suggest are due to either deeply buried AGN or hyper star clusters. This is also consistent with the high column densities of H_2, higher than 10^{25} cm^{-2}, which they found towards the cores of both galaxies. In Arp 220 they detected an outflow while in NGC 4418 there is an apparent inflow onto the nucleus. A strong enhancement of ^{18}O with a ^{16}O/^{18}O ratio of $70 - 130$ is inferred in Arp 220 while NGC 4418 seems to have a ratio similar to the solar system isotopic ratio. The authors suggest that the differences in kinematics and ^{18}O enhancement in the two galaxies are due to different evolutionary stages where the activity in Arp 220 is in a later stage and both galaxies are in an earlier phase than Mrk 231. In contrast, Rangwala et al. (2011) performed dust modeling of Arp 220 based on continuum measurements from the SPIRE instrument and found a dust temperature of 66 K and a column density of H_2 of $\sim 10^{25}$ cm^{-2}. Both of these values are lower than those found by González-Alfonso et al. (2012), reflecting the fact that the highly excited lines of H_2O and OH probe a warm dust component close to the nucleus, while a single-temperature fit to the total continuum will also include colder and less dense regions further away from the source.

Combining *Herschel* spectroscopic observations of 29 local (U)LIRGs, including both starburst- and AGN-dominated sources, with radiative transfer models, González-Alfonso et al. (2015) found indications that strong OH 65 μm absorption lines and [C II] deficits are associated with warm ($T_{\rm dust} \gtrsim 60$ K) structures with high column densities ($N_{\rm H} \gtrsim 10^{24}$ cm^{-2}), probably confined to small regions around the central power source.

3.2 Interferometric observations at radio and (sub)mm wavelengths

As already mentioned, radiation at longer wavelengths is better able to penetrate the dusty cocoons surrounding the central regions of CONs, although a potential problem at radio wavelengths is free-free absorption from young star formation. At (sub)mm and radio wavelengths it is also possible to conduct ground-based observations in multiple atmospheric windows. Furthermore, the availability of interferometers at these wavelengths offers a tool to achieve much higher angular resolution than with single-dish telescopes, for which the CONs are essentially point-like sources.

3.2.1 Instruments used in this work

In Papers III and IV we use observations conducted with arrays of connected (sub)mm or radio telescopes, the interferometers. A thorough introduction to interferometry is beyond the scope of this thesis, but a few basic concepts should be mentioned before a short introduction to the interferometers used in this work (see Fig. 3.4).

For a single radio telescope, the achievable angular resolution is proportional to the ratio of the observed wavelength to the diameter of the antenna $\Theta \sim \lambda/D$. In order to achieve an angular resolution better than an arcsecond, a single-dish telescope observing at mm wavelengths would have to be several hundreds of meters in diameter, a problem that is even worse at longer wavelengths. For an interferometer, the angular resolution is instead proportional to the ratio of the observed wavelength to the maximum distance, or baseline, between two antennas $\Theta \sim \lambda/B_{\rm max}$. In this way, the angular resolution, but not the sensitivity, of a much larger telescope can be achieved with an array of smaller antennas. However, the high angular resolution comes at the expense of sensitivity to extended structures, as the largest angular scale that the interferometer is sensitive to depends on the minimum baseline between antennas. Due to this problem of "missing short spacings", emission from structures larger than $\Theta \sim \lambda/B_{\rm min}$ cannot be detected by an interferometer and are said to be resolved out.

The Submillimeter Array (SMA)

The SMA is an interferometer consisting of eight movable 6-meter antennas located at an altitude of 4080 m, close to the summit of Mauna Kea on the island of Hawaii, USA. Currently, each antenna has four receivers that together provide continuous coverage in the frequency range 182 to 420 GHz with simultaneous operation possible for some receiver pairs. The antennas can be arranged in four basic configurations with maximum baselines ranging between 25 and 509 m, offering angular resolutions between approximately $5''$ and $0.25''$ at 350 GHz. In Paper IV, we use the SMA in its extended configuration at 230 GHz, providing an angular resolution of approximately $1''$.

The *Karl G. Jansky* Very Large Array (VLA)

The VLA is an interferometer located at an altitude of 2100 m on the Plains of San Agustin in New Mexico, USA. It consists of 27 movable 25-meter antennas which can be arranged in four differently sized Y-shaped configurations with the minimum and maximum antenna separations spanning from 35 to 680 m and 1 to 36.4 km, respectively. With receivers providing continuous coverage at frequencies from 1.0 to 50 GHz as well as receivers operating at MHz-

frequencies, it can achieve a maximum resolution of $0.04''$. In Paper IV, we use it to observe at 6 GHz in the most extended A-configuration, providing an angular resolution of $0.33''$ and a largest angular scale of $8.9''$.

The Atacama Large Millimeter/submillimeter Array (ALMA)

ALMA is an interferometer consisting of 50 movable 12-meter antennas located at an altitude of 5000 m on the Chajnantor plateau in the Atacama desert in Chile. In addition, it also includes the Atacama Compact Array (ACA) consisting of twelve 7-meter antennas and four 12-meter antennas which can be used to image extended structures that are not well sampled by the 12-meter array. The frequency range of ALMA is divided into different bands which follow the atmospheric windows. Band 3, starting at 84 GHz, to band 10, ending at $\sim$950 GHz, are currently in operation. The 12-meter array can be arranged in different configurations with maximum baselines ranging between $\sim$150 m and $\sim$16 km, currently providing angular resolutions between $0.018''$ and $3.4''$. The ALMA observations of Paper III are taken at $\sim$350 GHz with a maximum baseline of 625 m, providing an angular resolution of $\sim 0.3''$. In Paper IV, we use archival ALMA data taken at 690 GHz in a configuration with a maximum baseline of 555.5 m, providing an angular resolution of $\sim 0.2''$.

3.2.2 Probing deeper into the compact nuclei by observing at longer wavelengths

At the submillimeter wavelengths observable from the ground, the dust surrounding CONs is considerably less optically thick than in the far-IR, a situation that improves further for millimeter and radio wavelengths. This makes it possible to probe deeper into the nuclei, and by using sensitive interferometers we are also able to get information about the spatial distribution of the radiation. In this section we give a brief summary of previous efforts to observe obscured nuclei at submillimeter to radio wavelengths. Although some examples of single-dish observations are included, the focus is on observations with high enough angular resolution to begin to resolve the $10 - 100$ pc scale regions of interest in CONs.

Already in the early 1990s, CO $J = 1 - 0$ observations with the Owens Valley millimeter-wave interferometer revealed large nuclear concentrations of molecular gas in many (U)LIRGs, with the highest surface densities found in the CONs Arp 299A, Arp 220, IRAS 17208-0014, and Zw 049.057 (Sargent & Scoville, 1991; Scoville et al., 1991; Planesas et al., 1991). After an expansion of the same array, Sakamoto et al. (1999) conducted CO $J = 1 - 0$ and continuum observations with a resolution of $0.5''$, and discovered counter-rotating gas disks with radii of $\sim$100 pc in the two nuclei of Arp 220. In recent years, measure-

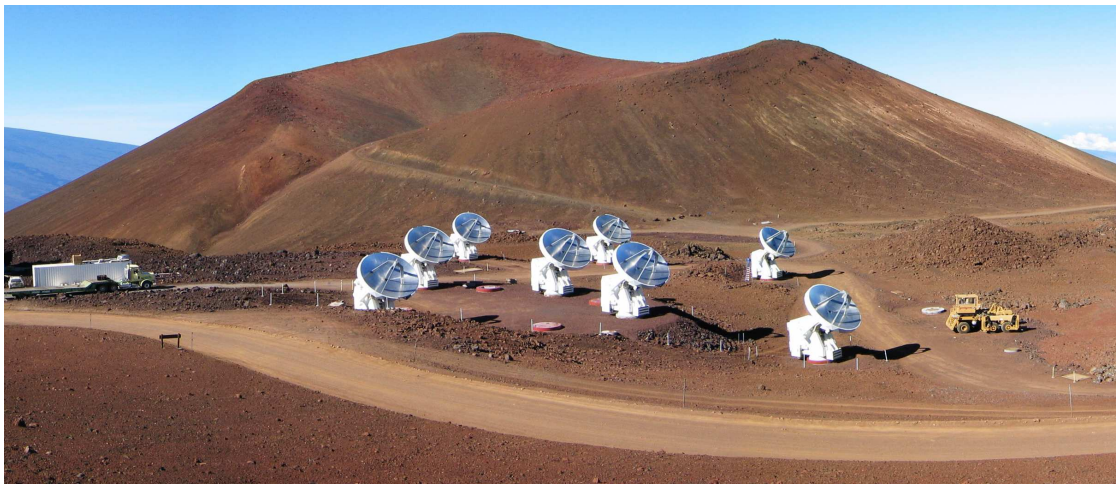

(a) View of the eight antennas of the SMA. Credit: J. Weintroub

(b) Panoramic view of the ALMA antennas. Credit: ESO

(c) Image of the antennas that make up the VLA. Credit: NRAO/AUI/NSF

Figure 3.4: Images of the three interferometric arrays used in the papers appended at the end of this thesis.

ments with interferometers such as the Plateau de Bure Interferometer (PdBI), later transformed into the Northern Extended Millimeter Array (NOEMA); the SMA; and ALMA have allowed (sub)mm imaging at high enough angular resolution to begin to resolve the actual CONs. With an angular resolution as high as $\sim 0.2''$, SMA and PdBI observations of CO $J = 2 - 1$ and $J = 3 - 2$, as well as the associated continuum, in Arp 220 revealed a bright core with a diameter of $50 - 80$ pc and a high column density of $N_{\rm H_2} \sim 10^{25}$ cm^{-2} (Downes & Eckart, 2007; Sakamoto et al., 2008). With submillimeter SMA observations of NGC 4418 at a similar resolution, Sakamoto et al. (2013) found evidence of a dusty core with a diameter of just ~ 20 pc embedded in a 100 pc scale concentration of molecular gas. The presence of a compact core is consistent with the results of Costagliola et al. (2013) who conducted millimeter and centimeter wavelength observations with the SMA and the Multi-Element Radio Linked Interferometer Network (MERLIN). Their analysis of the molecular excitation revealed a layered structure with three main temperature components (likely reflecting a steep temperature gradient) where the hottest component had an estimated size of 5 pc. In an ALMA spectral scan of NGC 4418, Costagliola et al. (2015) found bright emission from vibrationally excited HCN, HNC, and HC_3N, confirming the presence of a very compact core with diameter < 5 pc. Furthermore, 1.4 and 5.0 GHz radio observations with the European Very Long Baseline Interferometry Network (EVN) and MERLIN revealed a cluster of eight compact (< 8 pc) features within a region of 40 pc in the nucleus of NGC 4418 (Varenius et al., 2014). In their very long baseline interferometry (VLBI) observations of Arp 299A, also with the EVN, Pérez-Torres et al. (2009, 2010) detected a rich cluster of radio sources within the central 150 pc. They found that most of these sources can be attributed to a recent starburst, but based on the morphology, radio luminosity, spectral index, and ratio of radio-to-X-ray emission, they concluded that one of the regions is actually a low-luminosity AGN.

A promising probe of the central regions in CONs is the rotational lines of vibrationally excited HCN. The $v_2 = 1$ vibrational state of HCN is excited by radiation at 14 μm, but the rotational lines in the vibrationally excited state are emitted at (sub)millimeter wavelengths where the obscuring dust is less optically thick. The first extragalactic (sub)millimeter detection of such lines was reported by Sakamoto et al. (2010) who observed NGC 4418 with the SMA. Using ALMA and PdBI, Aalto et al. (2015) have since then detected intense emission from the HCN ($v_2 = 1$) $J = 3 - 2$ and $4 - 3$ lines in four CONs: IRAS 17208-0014, Arp 220, IC 860 and Zw 049.057. In all of these galaxies they also found evidence that the corresponding lines from the ground vibrational states of HCN and HCO^+ fail to probe the obscured nuclei due to strong self- and continuum absorption. Similar results were found by Martín et al. (2016) in their ALMA $0.5''$ resolution observations of HCN, HCO^+ and vibrationally excited HCN in Arp 220. While they found that the lines within the ground-vibrational state fail

to describe the central regions around the nuclei, the extent of the vibrationally excited HCN emission was marginally resolved to regions of 60×50 pc in both nuclei.

As mentioned in Sect. 2.3, some (U)LIRGS are known to host OH megamasers in which the main lines of the ground state Λ-doublet of OH exhibit strong masing (e.g. Baan et al., 1982, 1987; Baan & Haschick, 1987; Henkel & Wilson, 1990). For example, these maser lines have been used to trace molecular outflows (Baan et al., 1989), and observations at other radio wavelengths have revealed absorption lines of rotationally excited OH in some of the megamaser galaxies (e.g. Henkel et al., 1986, 1987). These results have generally been obtained using single-dish observations but follow-up VLBI observations of the maser emission have also been made. Examples include Arp 220 (Diamond et al., 1989; Lonsdale et al., 1998), III Zw 35 (Diamond et al., 1999; Pihlström et al., 2001; Parra et al., 2005), and IRAS 17208-0014 (Diamond et al., 1999; Momjian et al., 2006). In each of the two nuclei of Arp 220, as well as in III Zw 35 and IRAS 17208-0014, most of the maser emission originates in two distinct regions separated by some tens of pc. At least in the latter two galaxies this is consistent with clumpy ring-like structures with the two dominant maser regions marking the tangential points of the ring, where the amplification is indeed expected to be highest (Parra et al., 2005; Momjian et al., 2006).

Chapter 4

Introduction to appended papers

This chapter gives a short introduction to the appended papers, including a brief summary of the most important results and conclusions as well as possible ways to follow up on the findings presented in the papers.

4.1 Paper I: *Herschel* spectroscopic observations of the compact obscured nucleus in Zw 049.057

The LIRG Zw 049.057 is an edge-on early type disk galaxy with a compact radio core and an OH megamaser. It exhibits deep mid-infrared silicate absorption and a rich molecular spectrum. This paper is based on observations of Zw 049.057 taken with PACS as part of the *Herschel* OT2 program Hermolirg (PI: E. González-Alfonso) and with SPIRE as part of the OT key program Hercules (PI: P.P. van der Werf). These observations revealed emission and absorption of highly excited H_2O as well as absorption in rotational lines of both OH and ^{18}OH. Although not analyzed in the paper, absorption and emission in rotational lines of other light hydrides, as well as many lines from molecular ions, were also detected. Based on the detected OH and H_2O we have used the radiative transfer code described in González-Alfonso & Cernicharo (1997, 1999) to construct a model of the nuclear components of Zw 049.057.

We find that a minimum of two components are needed to account for the absorption lines of H_2O and OH in this galaxy. The high excitation lines require a compact, nuclear component with warm ($100 - 120$ K) dust and high abundances of both H_2O and OH. The estimated column density of H_2 towards this component may be as high as 10^{25} cm^{-2} and a buried X-ray source would be difficult to detect even in hard X-rays. In addition, the surface brightness of the component is between 10^{13} and 10^{14} L$_\odot$ kpc^{-2}, indicative of either a buried AGN or a very dense nuclear starburst as the power source. The ^{16}O/^{18}O ratio

of $75 - 150$ required to reproduce the ^{18}OH absorptions would place Zw 049.057 close to Arp 220 in the evolutionary scheme tentatively suggested by González-Alfonso et al. (2012) for NGC 4418, Arp 220, and Mrk 231. To also reproduce the emission lines in the submillimeter, an additional cooler ($40 - 50$ K) and less dense component is required. The presence of signatures of both in- and outflowing gas might indicate that the nucleus is in a stage of rapid evolution.

4.1.1 Future prospects

The *Herschel* observations also revealed emission and absorption of other light hydrides as well as many lines from molecular ions. Modeling of the molecular ions could for example provide important information about the oxygen chemistry in the ISM of Zw 049.057. Some of the absorption lines reported in this paper exhibit tentative in- and outflow signatures which we did not attempt to model. Further study of these features would provide information about the gas motions they are possibly tracing.

4.2 Paper II: Inflowing gas onto a compact obscured nucleus in Arp 299A: *Herschel* spectroscopic studies of H_2O and OH

The interacting system Arp 299 consists of two galaxies, IC 694 and NGC 3690, whose nuclei (Arp 299A and Arp 299B) and an overlap region (Arp 299C) are strong emitters of infrared and radio radiation. In this paper, we have used observations taken with the PACS and SPIRE instruments onboard *Herschel* to model the central regions of Arp 299A using the same radiative transfer code as in paper I. We find that Arp 299A, just as Zw 049.057, contains a compact obscured nucleus with warm (> 90 K) dust and high abundances of OH and H_2O, with a ratio of OH to H_2O above unity. The high surface brightness ($> 10^{13}$ $L_\odot$ kpc^{-2}) of this component indicates that the nuclear power source is a buried AGN, a compact starburst, or a combination of both. The high ratio of OH to H_2O suggests that ion-neutral chemistry is important, and is consistent with models of dense molecular gas irradiated by X-rays or cosmic rays. Unlike in Zw 049.057 (paper I), no ^{18}O isotopologues are detected in Arp 299A, and our models indicate that the ^{16}O/^{18}O ratio must be rather high with a lower limit of 400. This is higher than in Zw 049.057, possibly indicating that the starburst activity in Arp 299A is younger than in Zw 049.057. Redshifted absorption lines in one of the ground state OH transitions indicate an extended inflow of low-excited gas, possibly offering an alternative explanation to the high ^{16}O/^{18}O ratio by supplying the nucleus with relatively unprocessed gas. In addition to the core component, a more extended component with slightly cooler dust ($70 - 90$ K) is required to account for the low-excited lines as well as the emission

lines at the submillimeter wavelengths.

4.2.1 Future prospects

A rudimental model of a hemispherical inflow was used to show that the redshifted feature in the ground state OH doublet could indeed be caused by an inflow of low-excited gas. More detailed modeling could confirm this and possibly give a more realistic figure for the mass inflow rate toward the nucleus. In addition, interferometric studies of, for example, low J CO transitions or the hyperfine transitions of OH could be used in order to study the spatial distribution of the inflowing gas and how it is related to the nucleus. It would also be helpful to study the nucleus directly with high resolution interferometric measurements at longer wavelengths where the radiation can penetrate the obscuring dust better. Together with the observations of gas kinematics on larger scales, this could provide important information about how gas from the host or the interacting galaxy is transported to the compact obscured nucleus.

4.3 Paper III: The dense molecular gas and nuclear activity in the ULIRG IRAS 13120-5453

The ULIRG IRAS 13120-5453 is a post-merger system, optically classified as a Seyfert 2, where reprocessed radiation from the AGN and a starburst is believed to cause the high infrared luminosity (2.1×10^{12} $L_\odot$). X-ray observations are consistent with the presence of a Compton thick AGN that contributes approximately one fifth of the infrared luminosity. In this paper, we have used ALMA band 7 observations of the dense gas tracers HCN $v_2 = 0, 1$, $J = 4 - 3$, HCO^+ $J = 4 - 3$, and CS $J = 7 - 6$ as well as the 333 GHz continuum emission. We have also used *Herschel* far-infrared and submillimeter observations of H_2O in order to make similar, although less detailed, models as in papers I and II. My contribution in this work has been the data reduction and modeling of these far-infrared and submillimeter *Herschel* observations.

No HCN $v_2 = 1f$, $J = 4 - 3$ emission was detected in IRAS 13120-5453, and the ratio of the $v = 0$ to the $v_2 = 1f$ lines is at least ten times higher than the ratio measured towards galaxies with detectable vibrationally excited HCN. Two out of ten observed far-IR H_2O lines were detected in absorption and five out of ten observed submillimeter lines were detected in emission. The strengths of the observed H_2O transitions are consistent with a single component with a moderate dust temperature of $40 - 60$ K. The 333 GHz continuum was marginally resolved and the results imply a starburst diameter of 500 pc with an IR surface luminosity of $\sim 5 \times 10^{12}$ $L_\odot$ kpc^{-2}.

Although IRAS 13120-5453 has some similarities with CONs, for example

the presence of a Compton-thick nucleus and a significant [C II] deficit, there are also important differences. The lack of vibrationally excited HCN emission together with the fact that the dust temperature and the IR surface luminosity are lower than what is inferred in CONs suggests that there is no compact obscured nucleus present in IRAS 13120-5453. This does not rule out the possibility that it has gone through a CON state, but in that case feedback from the central parts has likely already inflated the core gas distribution and diluted the nuclear star formation. A massive molecular outflow has indeed been detected in the OH absorption doublet at 119 μm in IRAS 13120-5453 by Sturm et al. (2011).

4.3.1 Future prospects

Although no compact obscured nucleus was found in IRAS 13120-5453, the notion that we might be observing it in a post-CON phase still makes it an interesting object. Especially interesting in the context of CONs are the feedback processes that are inflating and clearing the nuclear ISM, and how they are related to the activity in the core of the galaxy. Signatures of outflowing dense molecular gas in the form of line wings were seen in both the HCN and HCO^+ $J = 4 - 3$ lines. We also found an enhanced HCN/HCO^+ ratio in the $J = 4 - 3$ transition, peaking at a value of almost three at the position of the central starburst. However, due to the limited number of transitions observed, we cannot model the physical conditions in the dense gas. Future multi-transition observations of these species would allow for LVG modeling to determine properties such as the temperature, density, column density, and relative abundances in the outflowing gas as well as in the central starburst. Knowing the excitation conditions and abundances would allow for comparison with the conditions in CONs and possibly to test the idea that IRAS 13120-5453 has experienced a CON phase.

4.4 Paper IV: A hidden molecular outflow in the LIRG Zw 049.057

In this paper we revisit the LIRG Zw 049.057 which was observed in the far-infrared and submillimeter with *Herschel* in Paper I. The identification of a CON and the detection of possible signatures of both out- and inflowing gas led us to observe the galaxy with the SMA and VLA interferometers to try to spatially resolve the compact nucleus as well as the gas kinematics using CO $J = 2 - 1$ and the rotationally excited OH 4.7 and 6 GHz lines as tracers. In addition, we used CO $J = 6 - 5$ and 690 GHz continuum data found in the ALMA archive. The angular resolution was, approximately, $1''$ (270 pc), $0.3''$ (80 pc), and $0.2''$

(50 pc) for the SMA, VLA, and ALMA observations.

Outflow signatures in the form of spatially unresolved blueshifted line wings were found in the OH absorption lines toward the nuclear radio continuum. Tentative line wings were also found in the CO $J = 2 - 1$ line toward the central arcsecond of the nucleus. The presence of outflowing CO gas was confirmed by the ALMA data, where the clearly detected blue- and redshifted line wings were seen to be spatially offset along an axis almost perpendicular to the overall rotation of the galaxy. In addition, the radio continuum image revealed a jet-like feature, also approximately perpendicular to the overall velocity gradient of the galaxy. This radio jet was also found to be aligned with a previously detected dust feature extending at least 500 pc from the center of the nucleus. Finally, a simple comparison of the apparent optical depths of the OH lines indicate that the excitation conditions in Zw 049.057 differ from those in other OH megamasers, possibly indicating that the galaxy is in a transition state in its megamaser activity.

4.4.1 Future prospects

It is still unclear if, and in that case how, the radio jet is related to the molecular outflow. In order to confirm this and study how both of these features are related to the nuclear activity, observations with better sensitivity and higher spatial resolution are required. At the time of writing, we have a C-rated ALMA proposal to observe CO $J = 2 - 1$ at a resolution of $< 0.2''$ to confirm and spatially resolve the tentative outflow. The proposal also includes observations of HCN $v_2 = 1f$, $J = 3 - 2$ at a resolution of $< 0.05''$ ($\sim$15 pc) to study the inner core of the galaxy and potentially trace the transition region between the environment closest to the SMBH and the larger scale host galaxy.

4.5 General results and future prospects

From Papers I-III (as well as previous efforts by González-Alfonso et al. (2012)) it is clear that radiative transfer modeling based on a combination of far-IR and submillimeter observations is a promising method to discover CONs. Although *Herschel* is no longer in operation, there are still data in the *Herschel* science archive that have not yet been analyzed. In particular, there are observations of the CON galaxies IRAS 17208-0014 and IRAS 11506-3851, taken as part of the Hermolirg program, that are still waiting for a detailed analysis. A full analysis of these data would for example allow us to determine if there is an enhancement of ^{18}O in these galaxies. Another interesting study would be to use radiative transfer modeling to simultaneously reproduce the far-IR OH absorptions and the megamaser OH emission from the galaxies where both have been observed.

In Paper IV, the fact that we are able to detect a molecular outflow, in a relatively small amount of time, using the 4.7 and 6.0 GHz lines of OH is fascinating. This might be a way to probe the nuclear acceleration region of molecular outflows in CONs, and thus find out how they are connected to the nuclear activity. An interesting follow-up would be to observe OH lines in higher rotationally excited states, at higher frequencies, to try to map the outflow with higher spatial resolution. Another intriguing result is the seemingly different excitation conditions in Zw 049.057 as compared to other OH megamasers. It would be interesting to conduct a wider study of rotationally excited OH in CONs, and other OH megamasers, in order to make a more detailed comparison of the excitation conditions and try to understand how they differ between different sources.

Bibliography

Aalto, S. 2013, in IAU Symposium, Vol. 292, IAU Symposium, ed. T. Wong & J. Ott, 199–208

Aalto, S., Garcia-Burillo, S., Muller, S., et al. 2012, A&A, 537, A44

Aalto, S., Martín, S., Costagliola, F., et al. 2015, A&A, 584, A42

Aalto, S., Monje, R., & Martín, S. 2007, A&A, 475, 479

Andrews, B. H. & Thompson, T. A. 2011, ApJ, 727, 97

Antonucci, R. 1993, ARA&A, 31, 473

Baan, W. A. & Haschick, A. D. 1987, ApJ, 318, 139

Baan, W. A., Haschick, A. D., & Henkel, C. 1989, ApJ, 346, 680

Baan, W. A., Henkel, C., & Haschick, A. D. 1987, ApJ, 320, 154

Baan, W. A., Wood, P. A. D., & Haschick, A. D. 1982, ApJ, 260, L49

Barnes, J. E. & Hernquist, L. E. 1991, ApJ, 370, L65

Bayet, E., Viti, S., Williams, D. A., & Rawlings, J. M. C. 2008, The Astrophysical Journal, 676, 978

Bernes, C. 1979, A&A, 73, 67

Brightman, M. & Ueda, Y. 2012, MNRAS, 423, 702

Burlon, D., Ajello, M., Greiner, J., et al. 2011, ApJ, 728, 58

Chapman, S. C., Blain, A. W., Smail, I., & Ivison, R. J. 2005, ApJ, 622, 772

Cicone, C., Maiolino, R., Sturm, E., et al. 2014, A&A, 562, A21

Comastri, A., Setti, G., Zamorani, G., & Hasinger, G. 1995, A&A, 296, 1

Condon, J. J., Huang, Z.-P., Yin, Q. F., & Thuan, T. X. 1991, ApJ, 378, 65

Costagliola, F. & Aalto, S. 2010, A&A, 515, A71

Costagliola, F., Aalto, S., Rodriguez, M. I., et al. 2011, A&A, 528, A30

Costagliola, F., Aalto, S., Sakamoto, K., et al. 2013, A&A, 556, A66

Costagliola, F., Sakamoto, K., Muller, S., et al. 2015, A&A, 582, A91

Courvoisier, T. J.-L. 2013, High Energy Astrophysics

Davies, R. I., Müller Sánchez, F., Genzel, R., et al. 2007, ApJ, 671, 1388

Diamond, P. J., Lonsdale, C. J., Lonsdale, C. J., & Smith, H. E. 1999, ApJ, 511, 178

Diamond, P. J., Norris, R. P., Baan, W. A., & Booth, R. S. 1989, ApJ, 340, L49

Downes, D. & Eckart, A. 2007, A&A, 468, L57

Elitzur, M. 2012, ApJ, 747, L33

Fabian, A. C. 1999, MNRAS, 308, L39

Fabian, A. C., Barcons, X., Almaini, O., & Iwasawa, K. 1998, MNRAS, 297, L11

Fabian, A. C., Celotti, A., & Erlund, M. C. 2006, MNRAS, 373, L16

Falstad, N., González-Alfonso, E., Aalto, S., & Fischer, J. 2017, A&A, 597, A105

Falstad, N., González-Alfonso, E., Aalto, S., et al. 2015, A&A, 580, A52

Ferrarese, L. & Merritt, D. 2000, ApJ, 539, L9

Feruglio, C., Maiolino, R., Piconcelli, E., et al. 2010, A&A, 518, L155

Fischer, J., Sturm, E., González-Alfonso, E., et al. 2010, A&A, 518, L41

García-Burillo, S., Combes, F., Usero, A., et al. 2015, A&A, 580, A35

García-Burillo, S., Combes, F., Usero, A., et al. 2014, A&A, 567, A125

Gilli, R., Comastri, A., & Hasinger, G. 2007, A&A, 463, 79

Gonzalez-Alfonso, E. & Cernicharo, J. 1993, A&A, 279, 506

González-Alfonso, E. & Cernicharo, J. 1997, A&A, 322, 938

González-Alfonso, E. & Cernicharo, J. 1999, ApJ, 525, 845

González-Alfonso, E., Fischer, J., Aalto, S., & Falstad, N. 2014, A&A, 567, A91

González-Alfonso, E., Fischer, J., Bruderer, S., et al. 2013, A&A, 550, A25

González-Alfonso, E., Fischer, J., Graciá-Carpio, J., et al. 2012, A&A, 541, A4

González-Alfonso, E., Fischer, J., Isaak, K., et al. 2010, A&A, 518, L43

González-Alfonso, E., Fischer, J., Spoon, H. W. W., et al. 2017, ApJ, 836, 11

González-Alfonso, E., Fischer, J., Sturm, E., et al. 2015, ApJ, 800, 69

González-Alfonso, E., Smith, H. A., Ashby, M. L. N., et al. 2008, ApJ, 675, 303

González-Alfonso, E., Smith, H. A., Fischer, J., & Cernicharo, J. 2004, ApJ, 613, 247

Gould, R. J. & Salpeter, E. E. 1963, ApJ, 138, 393

Guilloteau, S. & Baudry, A. 1981, A&A, 97, 213

Henkel, C., Guesten, R., & Baan, W. A. 1987, A&A, 185, 14

Henkel, C., Guesten, R., & Batrla, W. 1986, A&A, 168, L13

Henkel, C. & Wilson, T. L. 1990, A&A, 229, 431

Hollenbach, D. & Salpeter, E. E. 1971, ApJ, 163, 155

Hopkins, P. F., Murray, N., & Thompson, T. A. 2009, MNRAS, 398, 303

Hughes, D. H., Serjeant, S., Dunlop, J., et al. 1998, Nature, 394, 241

Ibar, E., Sobral, D., Best, P. N., et al. 2013, MNRAS, 434, 3218

Lindberg, J. E., Aalto, S., Costagliola, F., et al. 2011, A&A, 527, A150

Lonsdale, C. J., Farrah, D., & Smith, H. E. 2006, Ultraluminous Infrared Galaxies, ed. J. W. Mason, 285

Lonsdale, C. J., Lonsdale, C. J., Diamond, P. J., & Smith, H. E. 1998, ApJ, 493, L13

Lusso, E., Hennawi, J. F., Comastri, A., et al. 2013, ApJ, 777, 86

Magorrian, J., Tremaine, S., Richstone, D., et al. 1998, AJ, 115, 2285

Martín, S., Aalto, S., Sakamoto, K., et al. 2016, A&A, 590, A25

Martín, S., Krips, M., Martín-Pintado, J., et al. 2011, A&A, 527, A36

Mathis, J. S., Rumpl, W., & Nordsieck, K. H. 1977, ApJ, 217, 425

Merloni, A., Bongiorno, A., Brusa, M., et al. 2014, MNRAS, 437, 3550

Mihos, J. C. & Hernquist, L. 1996, ApJ, 464, 641

Momjian, E., Romney, J. D., Carilli, C. L., & Troland, T. H. 2006, ApJ, 653, 1172

Moorwood, A. F. M. 1996, Space Sci. Rev., 77, 303

Murray, N., Quataert, E., & Thompson, T. A. 2005, ApJ, 618, 569

Nakai, N., Hayashi, M., Handa, T., et al. 1987, PASJ, 39, 685

Neff, S. G. & Ulvestad, J. S. 2000, AJ, 120, 670

Noguchi, M. 1988, A&A, 203, 259

Omont, A. 2007, Reports on Progress in Physics, 70, 1099

Parra, R., Conway, J. E., Elitzur, M., & Pihlström, Y. M. 2005, A&A, 443, 383

Pereira-Santaella, M., Colina, L., García-Burillo, S., et al. 2016, A&A, 594, A81

Pérez-Torres, M. A., Alberdi, A., Romero-Cañizales, C., & Bondi, M. 2010, A&A, 519, L5

Pérez-Torres, M. A., Romero-Cañizales, C., Alberdi, A., & Polatidis, A. 2009, A&A, 507, L17

Peterson, B. M. 1997, An Introduction to Active Galactic Nuclei

Pihlström, Y. M., Conway, J. E., Booth, R. S., Diamond, P. J., & Polatidis, A. G. 2001, A&A, 377, 413

Planesas, P., Mirabel, I. F., & Sanders, D. B. 1991, ApJ, 370, 172

Prantzos, N., Aubert, O., & Audouze, J. 1996, A&A, 309, 760

Rangwala, N., Maloney, P. R., Glenn, J., et al. 2011, ApJ, 743, 94

Rolffs, R., Schilke, P., Wyrowski, F., et al. 2011, A&A, 529, A76

Rybicki, G. B. & Hummer, D. G. 1991, A&A, 245, 171

Rybicki, G. B. & Lightman, A. P. 1979, Radiative processes in astrophysics

Sakamoto, K., Aalto, S., Costagliola, F., et al. 2013, ApJ, 764, 42

Sakamoto, K., Aalto, S., Evans, A. S., Wiedner, M. C., & Wilner, D. J. 2010, ApJ, 725, L228

Sakamoto, K., Aalto, S., Wilner, D. J., et al. 2009, ApJ, 700, L104

Sakamoto, K., Scoville, N. Z., Yun, M. S., et al. 1999, ApJ, 514, 68

Sakamoto, K., Wang, J., Wiedner, M. C., et al. 2008, ApJ, 684, 957

Sanders, D. B. & Mirabel, I. F. 1996, ARA&A, 34, 749

Sanders, D. B., Scoville, N. Z., Young, J. S., et al. 1986, ApJ, 305, L45

Sanders, D. B., Soifer, B. T., Elias, J. H., et al. 1988, ApJ, 325, 74

Sargent, A. & Scoville, N. 1991, ApJ, 366, L1

Schwarz, M. P. 1984, MNRAS, 209, 93

Scoville, N. 2003, Journal of Korean Astronomical Society, 36, 167

Scoville, N. Z., Sargent, A. I., Sanders, D. B., & Soifer, B. T. 1991, ApJ, 366, L5

Seyfert, C. K. 1943, ApJ, 97, 28

Shields, G. A. 1999, PASP, 111, 661

Shlosman, I., Frank, J., & Begelman, M. C. 1989, Nature, 338, 45

Smail, I., Ivison, R. J., & Blain, A. W. 1997, ApJ, 490, L5

Sobolev, V. V. 1960, Moving envelopes of stars

Spinoglio, L., Malkan, M. A., Smith, H. A., González-Alfonso, E., & Fischer, J. 2005, ApJ, 623, 123

Sturm, E., González-Alfonso, E., Veilleux, S., et al. 2011, ApJ, 733, L16

Thompson, T. A., Quataert, E., & Murray, N. 2005, ApJ, 630, 167

Tielens, A. G. G. M. 2010, The Physics and Chemistry of the Interstellar Medium

Türler, M., Paltani, S., Courvoisier, T. J.-L., et al. 1999, A&AS, 134, 89

Turner, B. E. 1985, ApJ, 299, 312

Ueda, Y., Eguchi, S., Terashima, Y., et al. 2007, ApJ, 664, L79

Urry, C. M. & Padovani, P. 1995, PASP, 107, 803

van der Tak, F. F. S., Black, J. H., Schöier, F. L., Jansen, D. J., & van Dishoeck, E. F. 2007, A&A, 468, 627

Varenius, E., Conway, J. E., Martí-Vidal, I., et al. 2014, A&A, 566, A15

Veilleux, S., Meléndez, M., Sturm, E., et al. 2013, ApJ, 776, 27

Walter, F., Weiss, A., & Scoville, N. 2002, ApJ, 580, L21

Wardlow, J. L., Smail, I., Coppin, K. E. K., et al. 2011, MNRAS, 415, 1479

Wilson, T. L., Rohlfs, K., & Hüttemeister, S. 2009, Tools of Radio Astronomy (Springer-Verlag)